ESRIUM

Grant Agreement No. 101004181

Deliverable 5.3
Test result analysis report

H2020-SPACE-EGNSS-2019-2020

ACKNOWLEDGEMENT:

This project has received funding from the European GNSS Agency under the European Union's Horizon 2020 research and innovation programme under Grant Agreement No. 101004181.

ESRIUM – GA No. 101004181 EGNSS-ENABLED SMART ROAD INFRASTRUCTURE USAGE AND MAINTENANCE FOR INCREASED ENERGY EFFICIENCY AND SAFETY ON EUROPEAN ROAD NETWORKS	
D5.3 Test result analysis report	
Due date of deliverable:	30.11.2023
Date of submission:	07.12.2023
Lead beneficiary for this deliverable:	VIF
Authors:	Selim Solmaz, Florian Pölzlbauer, Karl Lambauer, Georg Nestlinger, Kailin Tong, Kenan Mujkic, Martin Rudigier, Roman Lesjak, Sussane Schweitzer, Jose Vallet, Gottfried Allmer
Quality Reviewer	Martina Uray
State:	Final
Version:	V2
Dissemination nature:	PUB
Project Officer:	Katarzyna PORZUC
Reviewer 1:	Josep Maria SALANOVA GRAU
Reviewer 2:	Gustavo OYERVIDES ZERRWECK

Project partners
JOANNEUM RESEARCH Forschungsgesellschaft mbH – Institute DIGITAL (JRD), ASFINAG Autobahnen- und Schnellstraßen-Finanzierungs-Aktiengesellschaft (ASF), Virtual Vehicle Research GmbH (VIF), Finnish Geospatial Research Institute (FGI) of the National Land Survey (NLS) of Finland, FH OO FORSCHUNGS & ENTWICKLUNGS GMBH (FHO), Evolit Consulting GmbH (EVO), NNG Software Developing and Commercial LLC (NNG), ENIDE SOLUTIONS .S.L (ENI), Politecnico di Milano (POL)
Abstract
ESRIUM is a multi-national project with the common goal to increase the safety and resource efficiency of mobility on the road. The key innovation will be formed by a homogeneous, accurate and recent digital map of road surface damage and road wear. Further addressed as “road wear map”, it will contain unique information, which is of value to multiple stakeholders: road operators will be able to lower the road maintenance effort by optimal planning. Further, road operators will be able to lower road wear and increase traffic safety especially for heavy vehicles: considering the market introduction of partly automated truck fleets and platoons, the precise track of these vehicles can be adjusted by communicating precise routing recommendations in- and cross-lane. Truck fleet operators following these recommendations can receive tolling benefits, and increase the general safety for their vehicle fleet. Especially with the increasing levels of autonomy, systems will utilize infrastructure support to handle the requirements of the automated driving task and additional external requests. In ESRIUM, these opportunities are addressed by utilizing C-ITS infrastructure and EGNSS based localization in planning the trajectories of such automated vehicles. Key to the ESRIUM innovation is a precision localization service, which provides reliable locations of road damages and of the vehicles using the roads. Considering a European-level business-case, only Galileo may provide such a service in homogeneous quality, even at very remote locations on the European continent.

TABLE OF CONTENTS

LIST OF TABLES

LIST OF FIGURES

EXECUTIVE SUMMARY

This document provides a thorough analysis of the experimental data obtained from the ESRIUM project's extensive test campaigns with a specific automated driving test vehicle. The main focus is on the evaluation and discussion of key aspects that are crucial for the further development of automated driving systems. The document explores the complex interaction of infrastructure-based automated driving using Cooperative Intelligent Transport Systems (C-ITS) and ADAS/AD functionalities. It describes specific demonstrations involving lane keeping, in-lane lateral offset adaptations, and lane changes, and provides insights into their collective impact on system performance. In addition, the analysis evaluates localization performance for the end user and provides a detailed examination of the accuracy and reliability of localization technologies. Further details of the localization system solution are described in the corresponding WP3 deliverables, with the focus of the current document being on the reference to automated driving use cases. In this context, the trajectory-following use case is also explored to shed light on the adaptability of the system in real-world driving scenarios. This document also evaluates the effectiveness of C-ITS communication in providing precise route recommendations and accurate localization information. Essentially, this report is a detailed and nuanced examination of experimental data collected during ESRIUM automated driving demonstration campaigns.

DOCUMENT REVISION

Version	Changes to content	Author	Status	Date
V1	Initial complete version of the deliverable from all partners	VIF, JRD, FGI, ASF	DRAFT	06.11.2023
V2	Updated version according to the external review comments	VIF, JRD	FINAL	30.11.2023

ACRONYMS USED

Acronym	Explanation
AD	Automated Driving
ADAS	Advanced Driver Assistance Systems
CAN	Controller Area Network
CDF	Cumulative Distribution Function
C-ITS	Cooperative Intelligent Transport Systems
DBW	Drive-By-Wire
EGNSS	European GNSS
EUC-002	ESRIUM Use Case - 2
GNSS	Global Navigation Satellite System
GPS	Global Positioning System
IVIM	In-Vehicle Infotainment Messages

NRS	Nearest Reference Station
NTRIP	Networked Transport of RTCM via Internet Protocol
OSNMA	Open Service Navigation Message Authentication
PVT	Position, Velocity and Time
RTCM	Radio Technical Commission for Maritime Services
RTCMEM	RTCM Extended Messages
RTK	Real-Time Kinematic
RSU	Road Side Unit
V2X	Vehicle to everything
VRS	Virtual Reference Station

SECTION 1: INTRODUCTION

ESRIUM is a multinational project focused on improving road safety and resource efficiency. The main innovation is a detailed "road wear map" highlighting road surface damage, offering valuable insights and opportunities for various stakeholders. Such a map enables optimal maintenance planning, reduces road wear, and enhances safety for road vehicles, particularly in automated fleets. ESRIUM utilizes Cooperative Intelligent Transport Systems (C-ITS) and the European Global Navigation Satellite System (EGNSS) for generating strategic routing recommendations and localization solutions.

To illustrate ESRIUM's core ideas and bolster the project's business cases, we implemented and showcased smart routing applications supported by infrastructure. Real-life demonstrations took place, featuring an automated demonstrator vehicle equipped with an EGNSS receiver for Galileo-based localization services. The demonstrations specifically highlighted C-ITS-assisted in-lane positioning and lane change maneuvers, utilizing road damage data. The strategic routing recommendations were broadcast through ASFINAG's C-ITS roadside units (RSUs).

Within WP5, the primary goal is to showcase the project's advantages through in-vehicle field demonstrations, specifically illustrating context-aware routing recommendations in the form of targeted use-case demonstrations. These efforts serve the dual purpose of demonstrating potential business cases utilizing the road-wear map information and in the form of dedicated infrastructure communications. Additionally, real-time measurement of the test vehicle's position is essential, requiring centimeter-level accuracy and high robustness to serve as input for Advanced Driver Assistance Systems (ADAS) and automated driving (AD) functions.

The current document serves as a comprehensive analysis of the experimental data meticulously collected through the various test campaigns conducted with the designated test vehicle. The primary focus lies in providing an in-depth examination and discussion of several key facets:

1. ***Infrastructure-Enabled Automated Driving System Analysis:***

Explain the details of automated driving system implemented, leveraging infrastructure support building upon the Deliverable D5.1. This includes a thorough exploration of Cooperative Intelligent Transport Systems (C-ITS) and the application of Advanced Driver (AD) functionalities such as lane keeping, in-lane lateral offset adjustments, and lane changes. The results of the measurement campaign from the perspective of the driving function performance are analyzed and detailed.

2. ***End-User Localization Solution Performance Analysis:***

A critical aspect covered in this analysis is the evaluation of end-user localization performance. This involves a meticulous examination of how effectively the system determines and maintains the precise location of the end user (that is the test vehicle), providing insights into the accuracy and reliability of localization technologies employed during the experimental phases.

3. ***Trajectory-Following Use-Case Analysis:***

The document provides a detailed exploration of the trajectory-following use-case. This involves a comprehensive examination of how well the test vehicle adheres to predefined trajectories, considering various driving scenarios. Insights gained from this analysis contribute significantly to understanding the system's responsiveness and adaptability in real-world driving conditions.

4. ***Assessment of C-ITS Communications for Routing Recommendations and Localization:***

An integral component of the analysis revolves around the effectiveness of C-ITS communication. The document meticulously evaluates the system's capability to provide precise routing recommendations and accurate localization information. This evaluation is crucial not only for understanding the system's performance but also for assessing its potential in enhancing overall driving safety and efficiency.

In essence, this document aims to provide a comprehensive and nuanced exploration of the experimental data, offering valuable insights into the various dimensions of automated driving, localization, trajectory-following, and C-ITS communication within the context of the conducted test campaigns.

The subsequent sections present the outcomes from various test campaigns conducted in the scope of WP5. In Section 2, we present the demonstration context of ESRIUM use case EUC-002 Scenario-1 and Scenario-2, involving an automated driving end-user vehicle on the Austrian motorway A2. The test description precedes the presentation of a visualization tool and representative plots derived from the resulting datasets. A discussion of the test run results and observations concludes this section. Moving on to Section 3, we present the results of the performance analysis of the end-user localization solutions, covering experiments conducted in Finland and Austria. Section 4 delves into the results and analysis of the trajectory following use case (EUC-002 Scenario-3). Finally, Section 5 outlines the implementations of C-ITS communication solutions for routing recommendation use case, as well as providing relevant details regarding the end-user localization solution of ESRIUM. Within this context, we elaborate on the data flow, communication hardware, and the handling of RTK correction data via RTCM(EM), including details and analysis.

It is finally noted that the business case study of the ESRIUM Business Case-2 (EBC-2), titled "Routing Recommendations based on the road wear map, provided via C-ITS messages," was previously covered in deliverables D2.4.1 and D2.4.2 within the scope of WP2. In WP5, a practical implementation and demonstration of the corresponding use case, EUC002, is conducted. The results presented in this document solely pertain to the technical implementation details rather than the business case analysis. Therefore, analyzing EBC-2 further based on the demonstration results is not the objective of this document.

SECTION 2: ANALYSIS OF THE INFRASTRUCTURE-ENABLED AUTOMATED DRIVING TESTS

The demonstration of use case EUC-002 Scenario-1 and Scenario-2 was performed at 27.06.2023 on a about 10 km long section of the Austrian motorway A2 between “Graz Ost” and “Lassnitzhöhe”:

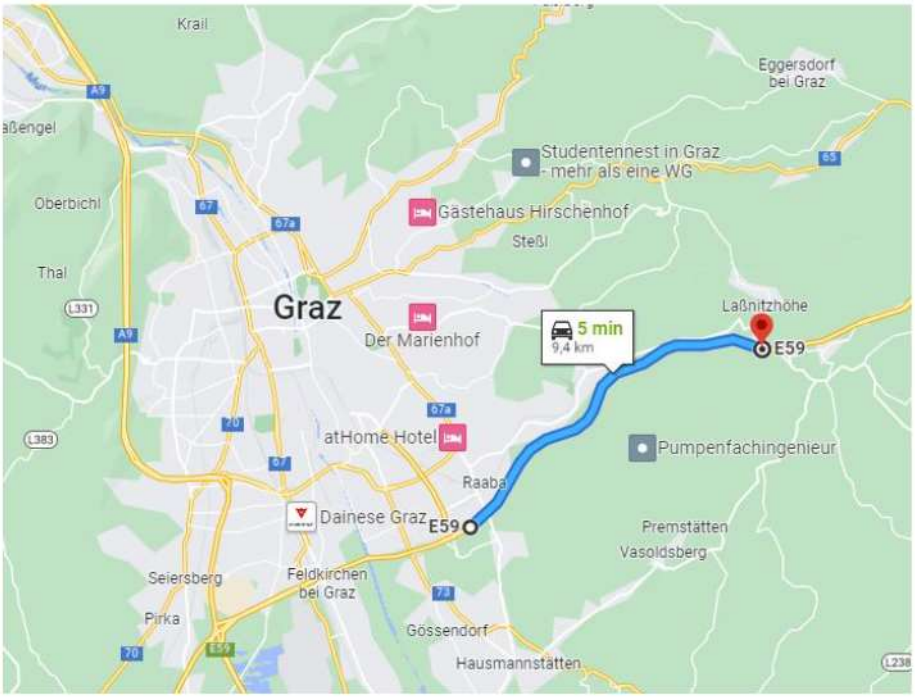

Figure 1: Section of the Austrian motorway A2 where the demo took place.

2.1. Logged data

For the analysis of the driving function performance w.r.t. the C-ITS recommendations, the following data was logged:

- Relevant vehicle CAN data (DBW status, speed, acceleration, angular rates, wheel speeds, …)
- Lane boundaries
- Detected objects
- GNSS data with several receivers
- C-ITS messages
- AD function internals

The last point (AD function internals) includes the lateral position of the vehicle w.r.t. the center of the current lane to easily assess the in-lane offset recommendations.

The logged data is stored in separate files according to the following structure, where "*" is a placeholder for the date and time:

- *_Controller.mat: Input/output and state signals of the speed and steering controller.
- *_GNSS.mat: On-board GPS and EGNSS receiver signals.
- *_Lanes.mat: Lane-marking signals (polynomial coefficients, quality, …).
- *_Objects.mat: Object list.
- *_Planner.mat: Input/output and parameter signals of the path planner.
- *_VhclSensors.mat: Vehicle sensor signals.

2.2. Test conditions and parameters

The test setup was designed according to

In total we performed 10 individual test runs with a desired speed of 90 kph, 110 kph and 130 kph, each of which lasting about 5 minutes:

Test run number	Desired velocity (kph)
1-4	90
5-7	110
8-10	130

Table 1: EUC-002 test parameters.

During the second test run, it started to rain heavily, and the Mobileye camera was no longer able to detect the lane markings. Therefore, this test was canceled and is excluded from the analysis.

Environmental conditions such as weather and traffic density varied naturally during the tests.

2.3. Test result visualization utilizing an interactive map framework

In order to make the test results available to a broader audience in an easy manner, we have generated interactive maps. These maps are attached to this report and can be viewed in a web-browser.

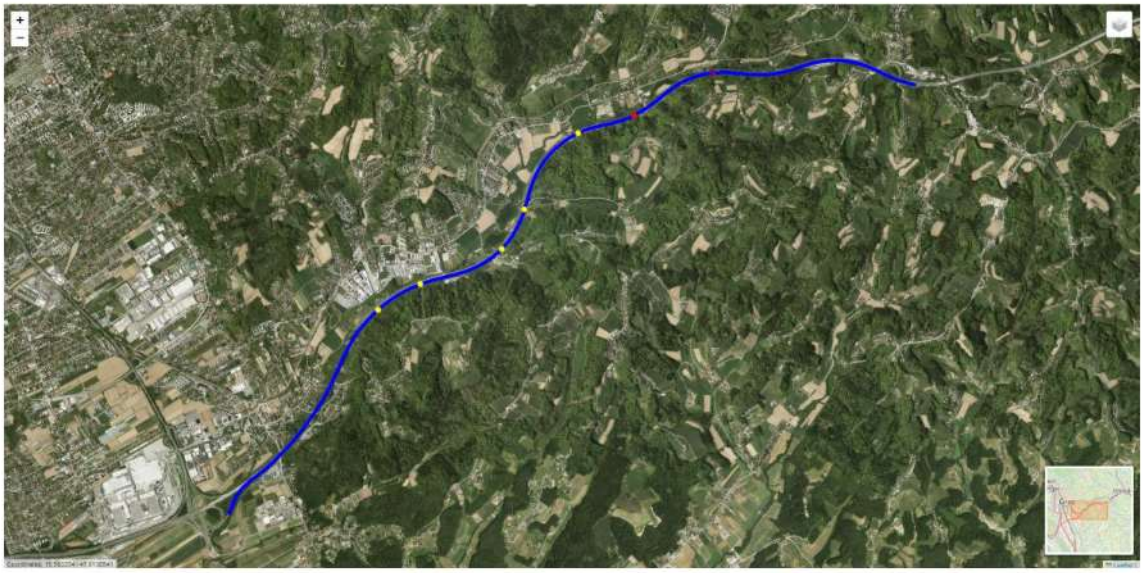

Figure 2: Map of test run results.

How to use the map?

The map can be used in a similar manner than other map-applications, such as google maps. By using the mouse, you can set the focus on the area of your interest. By using the +/- buttons (top left), you can zoom in/out.

By hovering over the layer-symbol (top right), a popup emerges. Here, you can select different background-tiles (such as satellite/areal-images). In addition, you can select different datasets which should be visualized on the map.

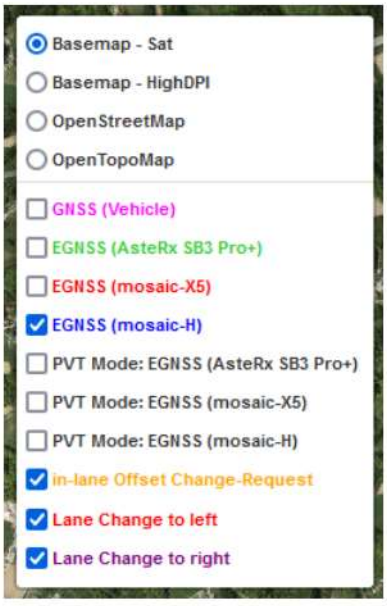

Figure 3: Map layers popup-menu.

The following background-tiles are available (see top of list):

Background	Description
Basemap – Sat	Satellite/Areal images (from Basemap)
Basemap – HighDPI	Symbolic map with high resolution (from Basemap)

OpenStreetMap	Symbolic map (from OpenStreetMap)
OpenTopoMap	Symbolic map including topology information (from OpenTopoMap)

Only one of them can be selected at a time.

The following datasets are available (see bottom of list):

Dataset	Description
GNSS (Vehicle)	Position of vehicle, according to on-board GPS receiver
EGNSS (AsteRx SB3 Pro+)	Position of vehicle, according to AsteRx SB3 Pro+ receiver
EGNSS (mosaic-X5)	Position of vehicle, according to mosaic-X5 receiver
EGNSS (mosaic-H)	Position of vehicle, according to mosaic-H receiver
PVT Mode: EGNSS (AsteRx SB3 Pro+)	PVT Mode of AsteRx SB3 Pro+ receiver
PVT Mode: EGNSS (mosaic-X5)	PVT Mode of mosaic-X5 receiver
PVT Mode: EGNSS (mosaic-H)	PVT Mode of mosaic-H receiver
in-lane Offset Change-Request	Position, at which an in-lane offset change (relative to middle of the current lane) was requested via C-ITS
Lane Change to left	Position, at which a lane-change towards left was performed
Lane Change to right	Position, at which a lane-change towards right was performed

Due to the large number of datasets, we have color-coded them on the map and in the menu. An arbitrary number of datasets can be selected at a time.

Due to the high accuracy of the EGNSS receivers, one can clearly identify the lane on which the vehicle was driving, and where the vehicle was performing a lane-change. However, the satellite/areal-images are not perfectly geo-referenced, thus one can notice a slight offset between satellite/areal-images and real-world lanes.

Figure 4: Position-track of vehicle driving on the 2nd lane.

When you click on a point, a popup emerges. Here details of the dataset for that particular location are shown.

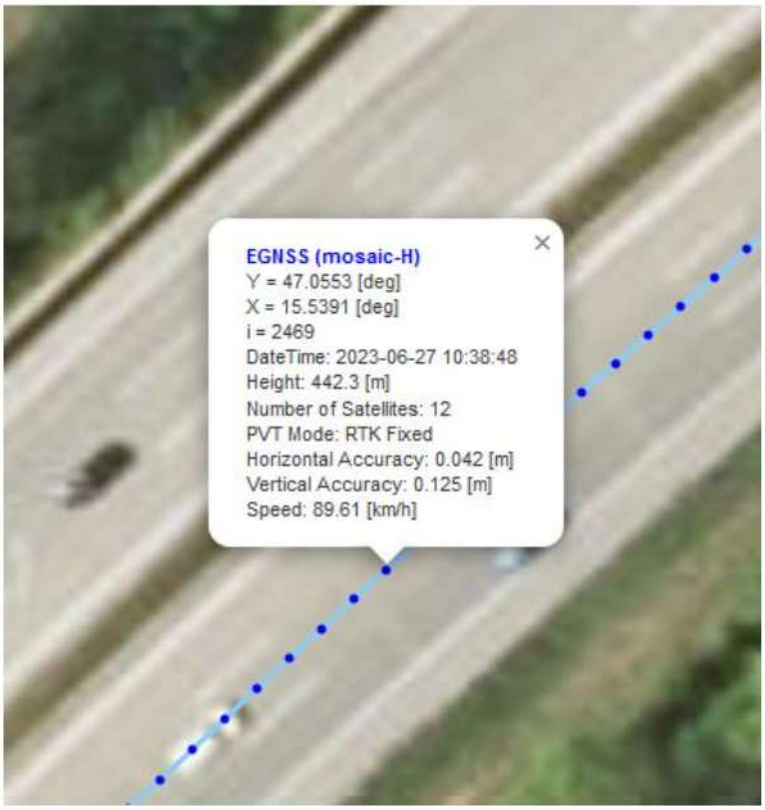

Figure 5: Details popup-menu for datapoint.

When you click on the line between points, another popup emerges. Here, the overall timeplot of the test run is shown.

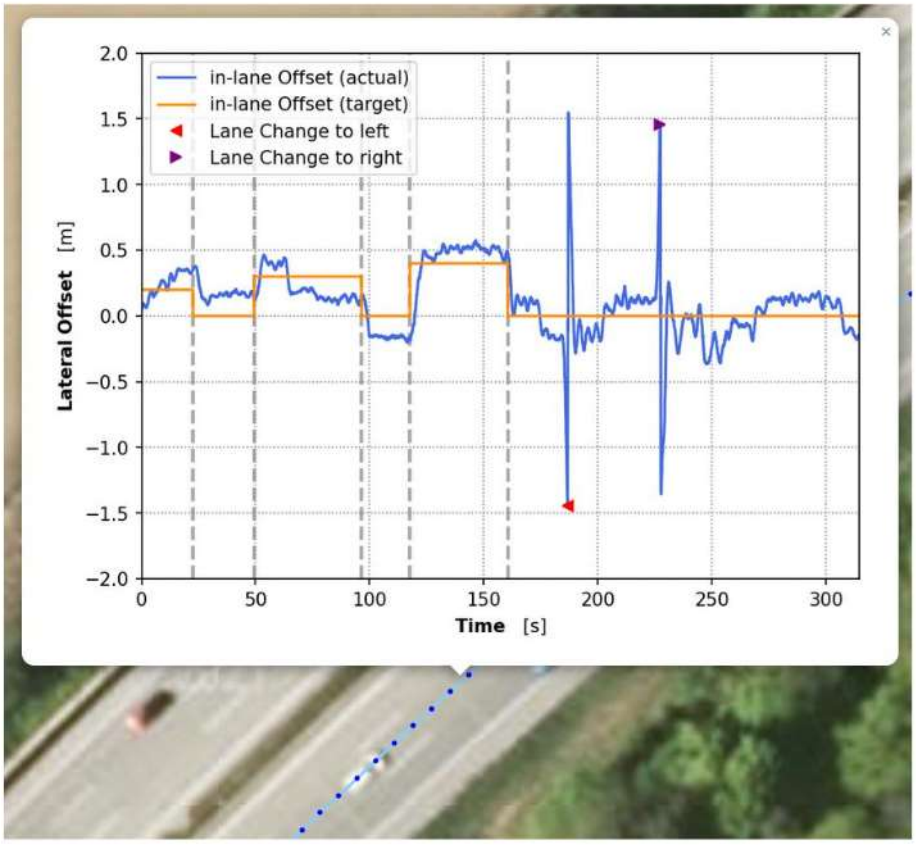

Figure 6: Details popup-menu for line.

Insight concerning EGNSS accuracy

During our test runs, the car was passing under several structures (bridges and gantries). By looking at the PVT-Mode of the EGNSS-tracks, we could identify that these structures hurt the PVT mode. The PVT mode switched away from “RTK Fixed” to “RTK Float” or “Differential” or “Standalone”. Figure 7 shows the effect of a gantry, while Figure 8 shows the combined effect of a gantry and bridge.

Figure 7: PVT Mode when driving under gantries.

Figure 8: PVT Mode behavior when passing a gantry followed by a bridge.
Green: RTK-fixed solution. Purple: RTK-float solution. Blue: stand-alone solution (SPP).

During these short phases, where the EGNSS-receiver loses the "RTK Fixed" status, the horizontal accuracy was getting very bad (up to 19m). Figure 9 shows the horizontal accuracy in log2 scaling of the EGNSS-receivers during test run 1. We can see that the accuracy significantly decreases at 35s, 256s, 304s, and 311-317s. These are the times, where the vehicle was just passing first underneath a gantry and then a bridge (driving in the image from left to right). Due to the gantry the GNSS receiver shortly loses the track to the satellite, typically cycle slips occur and as a result, the RTK-fixed solution (green dots) is lost. It falls back to an RTK-float solution (purple dots). Typically, after some more meters, an RTK-fixed solution would be achieved again. Within this scenario, this was not possible due to the following bridge where the tracking of all line-of-sight signals is lost for a moment. As a result, the solution falls back to the stand-alone (single point position, SPP) solution (blue dots), which is based on code pseudorange measurements only. Most probably, also some multipath signals are received. Surprisingly, the dotted line does not show significant deviations. It can be assumed that the navigation filter in the GNSS receiver assumes a quite constant (linear) movement where the error can be kept within a few meters, which cannot be identified due to the scale of the image. As soon as the line-of-sight to the satellite is given again, the GNSS receiver starts tracking the carrier phase again leading after a short moment to RTK-float solution (purple dots) and then RTK-fixed solution (green dots).

For automated driving applications, such situations may be critical. Thus, solutions for overcoming these situations are needed. One possible solution may be the integration of a IMU (inertial measurement unit), which can extrapolate the position of the vehicle, based on the measurements of acceleration.

Summarizing, already gantries shortly interrupt the reception of the GNSS signals leading in a significant decrease in the localization accuracy. Gantries in future will exist on a regular base (maybe every one or two kilometers for C-ITS RSUs, toll control, speed and distance measurements, and traffic signs indicating directions). In addition, we will have bridges, which all influences the GNSS accuracy significantly. This problem cannot be solved by GNSS only. Solutions exist by means of MEMS IMUs (inertial measurement units) and visual odometry (camera or LiDAR-based) but

currently, the prices for cars might still be not appropriate. The authors of this report are quite convinced that soon, solutions will be on the market.

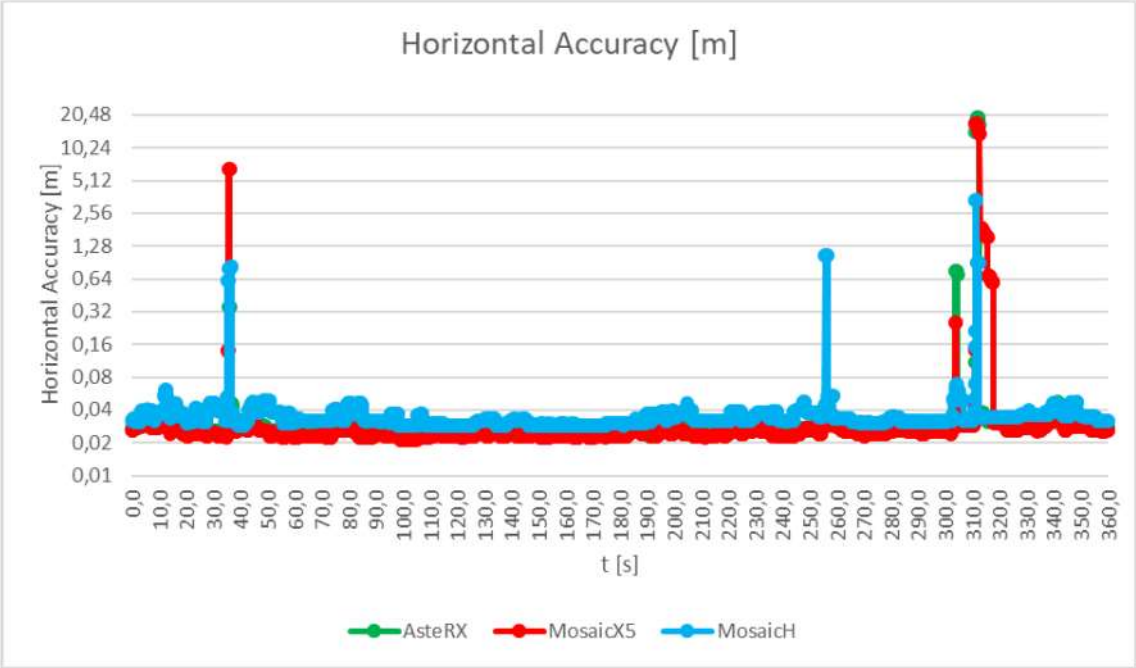

Figure 9: Horizontal accuracy measure estimated by the Septentrio (E)GNSS receivers (y-axis is scaled in log2).

The average accuracy reported by the different EGNSS receivers is as follows:

EGNSS receiver	average horizontal accuracy
Septentrio AsteRX SB3 Pro+	2.5 cm
Septentrio Mosaic X5	2.5 cm
Septentrio Mosaic H	3.5 cm

2.4. Test results

This section presents a graphical evaluation of the EUC-002 demonstrations, where the individual plots have the following meaning:

- The first row shows the covered path of the test vehicle where the AD function was enabled, i.e., the vehicle was driving autonomously. If the AD function was disabled, either manually by the driver or automatically due to e.g., insufficient lane marking detection, this is indicated by interrupted lines. E.g., Figure 10 shows four individual paths.
- The second row shows the status of the AD function being either ON (1) or OFF (0).
- The third row shows the desired velocity, which is constant for each test run, as well as the actual velocity. Due to a construction site blocking the leftmost lane, the desired speed could not be reached during approximately the first half of each test run.
- Finally, the fourth row shows the lateral offset of the vehicle with respect to the centerline of the current lane as well as the desired offset as encoded in the C-ITS message. A positive offset means that the vehicles look-ahead point is to the left of the centerline. C-ITS triggered lane changes were performed at the end of each test run and are indicated by a double-peak spark (decreasing lateral offset and switching sign to positive for a lane change to the left, vice versa for a lane change to the right). The corresponding relevance zones of the IVIM-message were filled with light colored areas. The yellow area indicates that the test vehicle

is in the relevance zone 1 of the IVIM, where the automated vehicle is requested to leave the rightmost lane due to oncoming road damage. The magenta area marks relevance zone 2, where the automated vehicle is requested to avoid the rightmost lane. The red area indicates relevance zone 2, where the automated vehicle is allowed to use all lanes according to the traffic.

2.4.1. Desired speed of 90 kph

Initially, the desired speed was set to 85 kph due to a temporary speed limit.

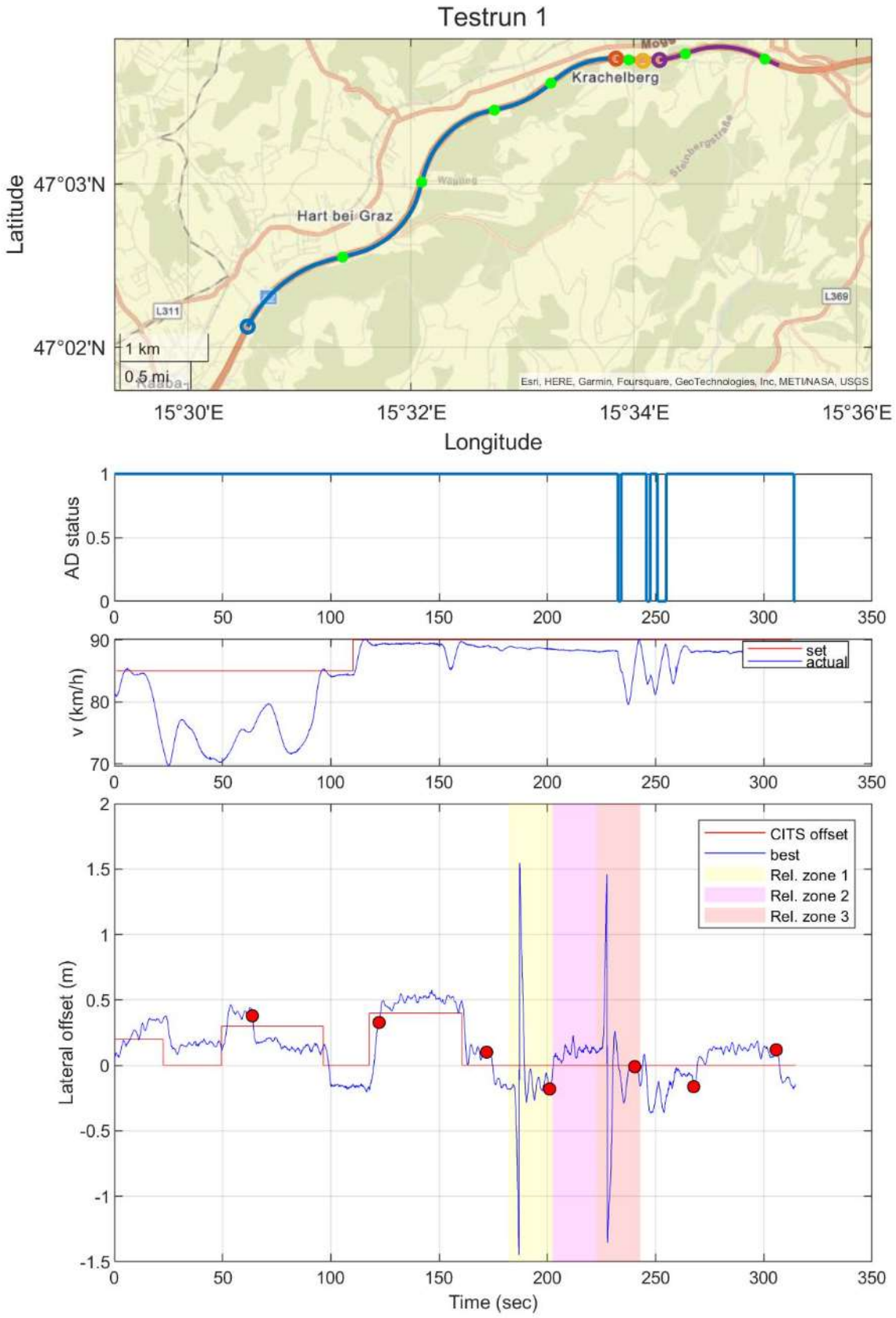

Figure 10: Test run 1 at 90 kph.

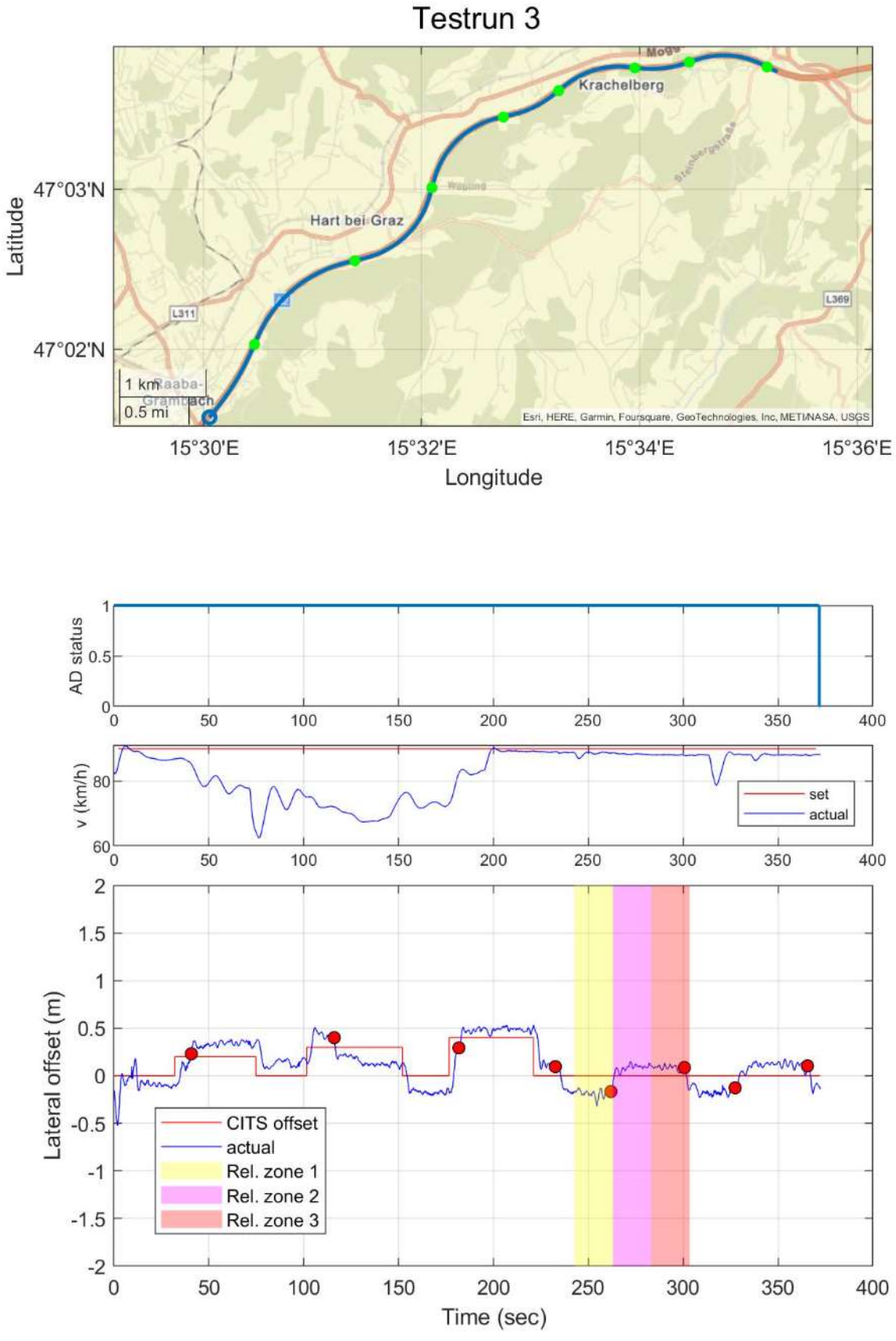

Figure 11: Test run 3 at 90 kph.

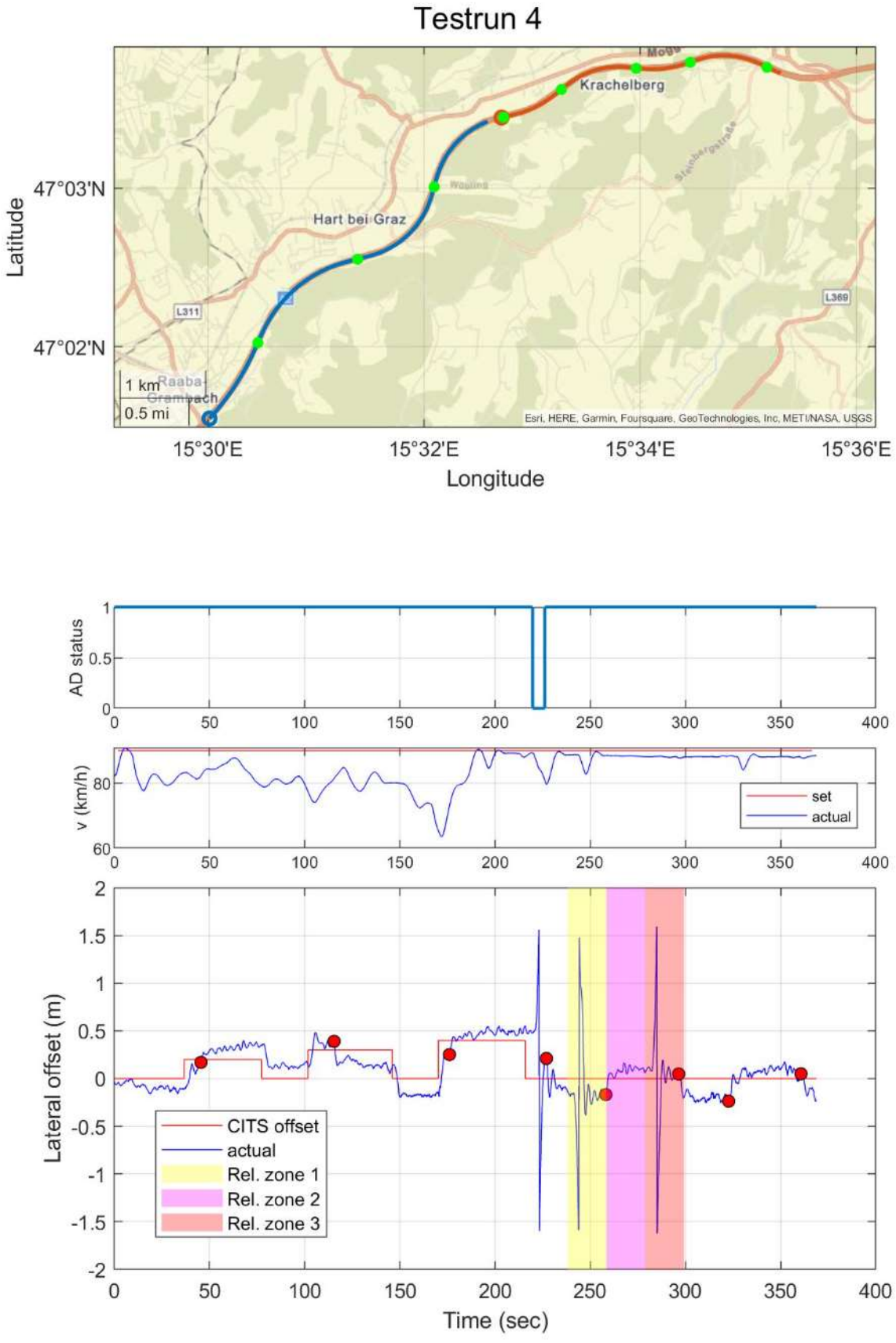

Figure 12: Test run 4 at 90 kph.

2.4.2. Desired speed of 110 kph

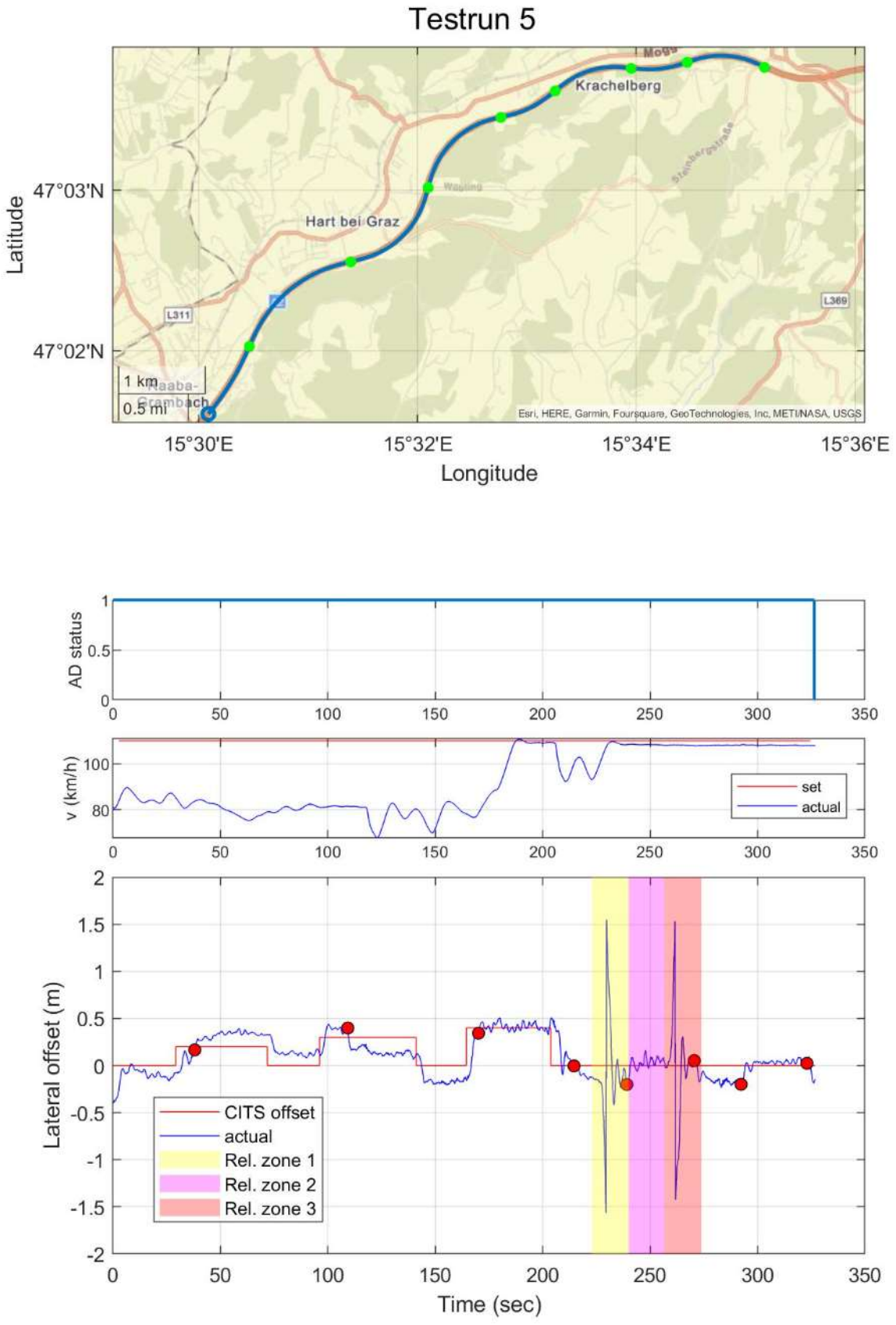

Figure 13: Test run 5 at 110 kph.

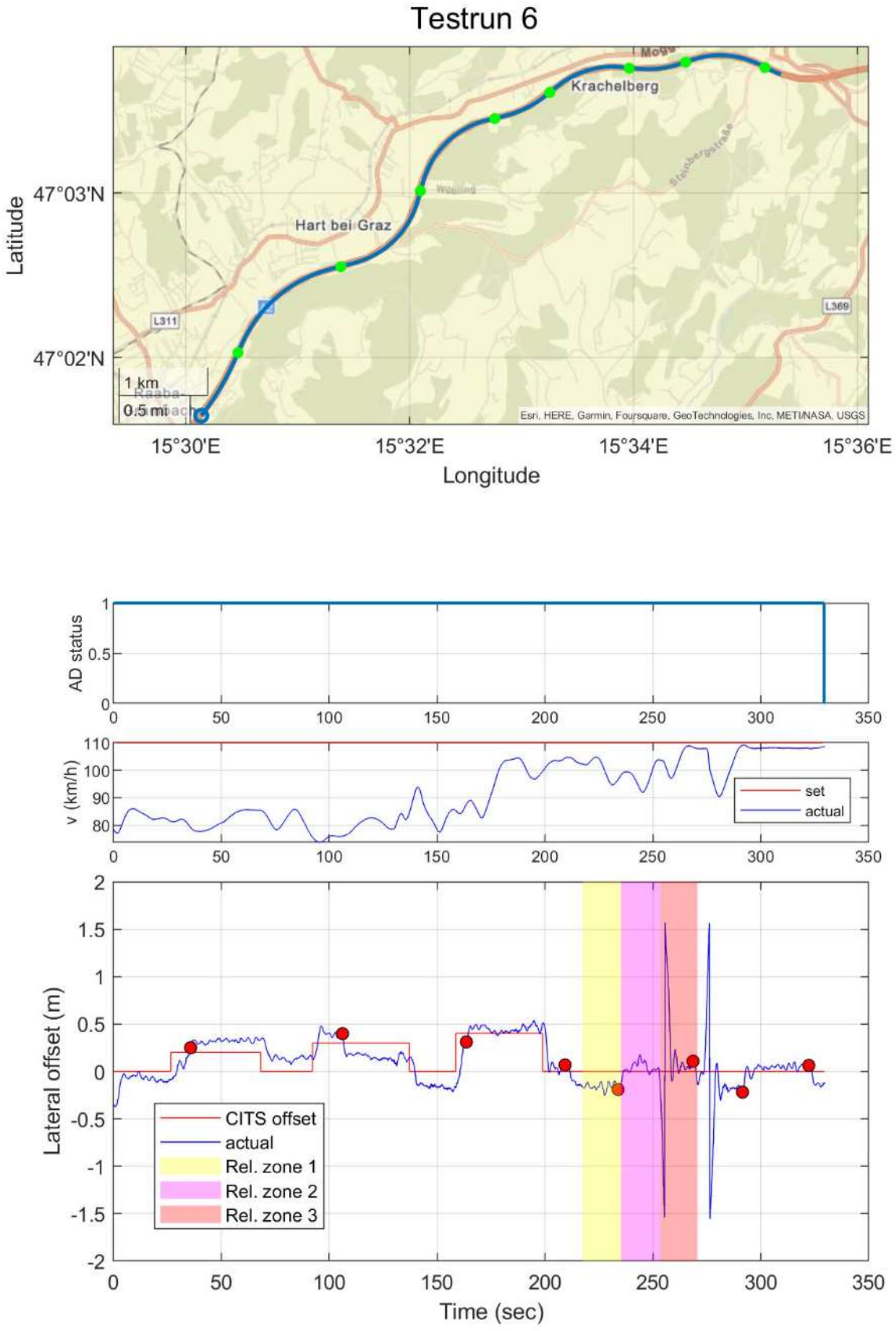

Figure 14: Test run 6 at 110 kph.

2.4.3. Desired speed of 130 kph

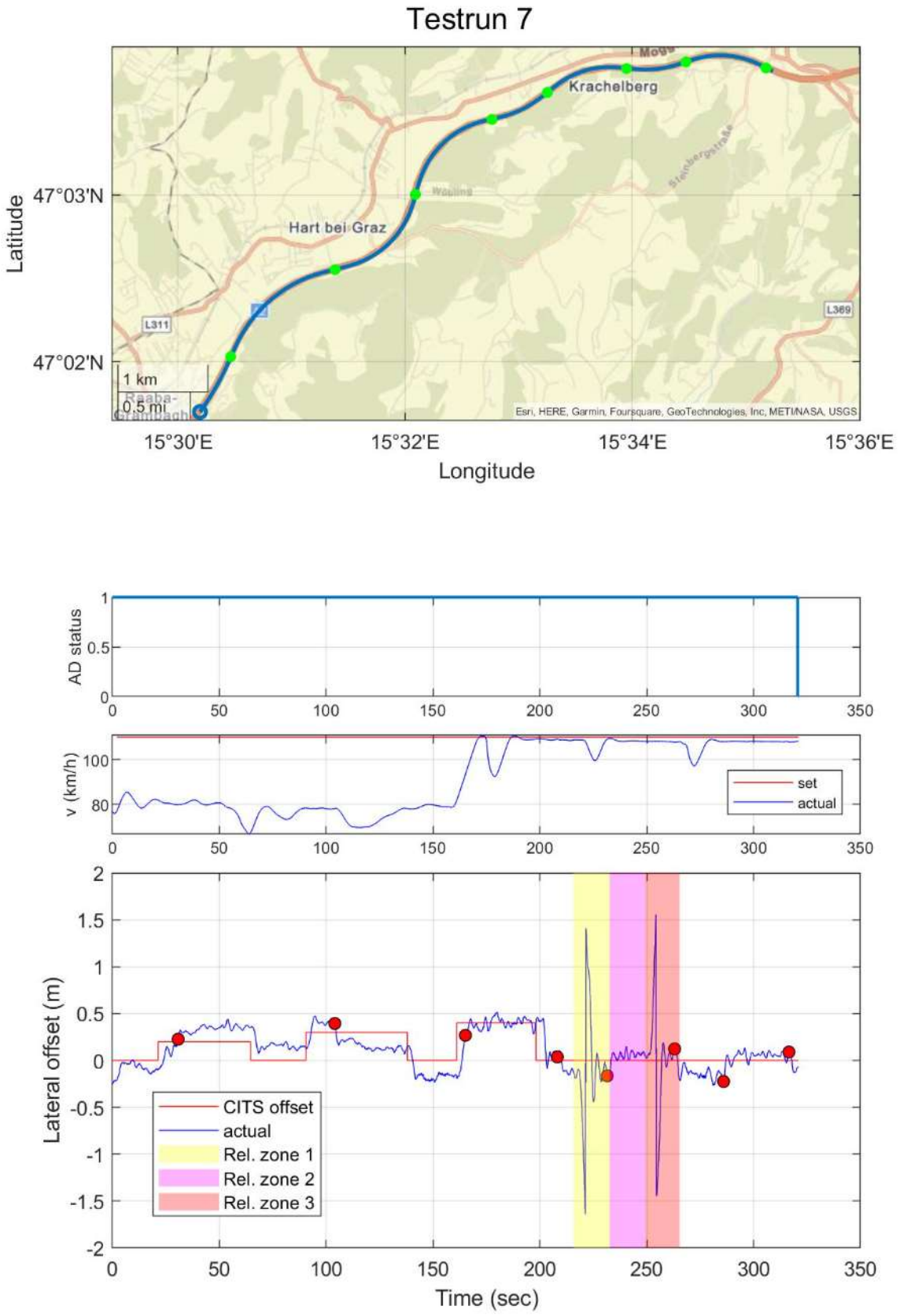

Figure 15: Test run 7 at 110 kph.

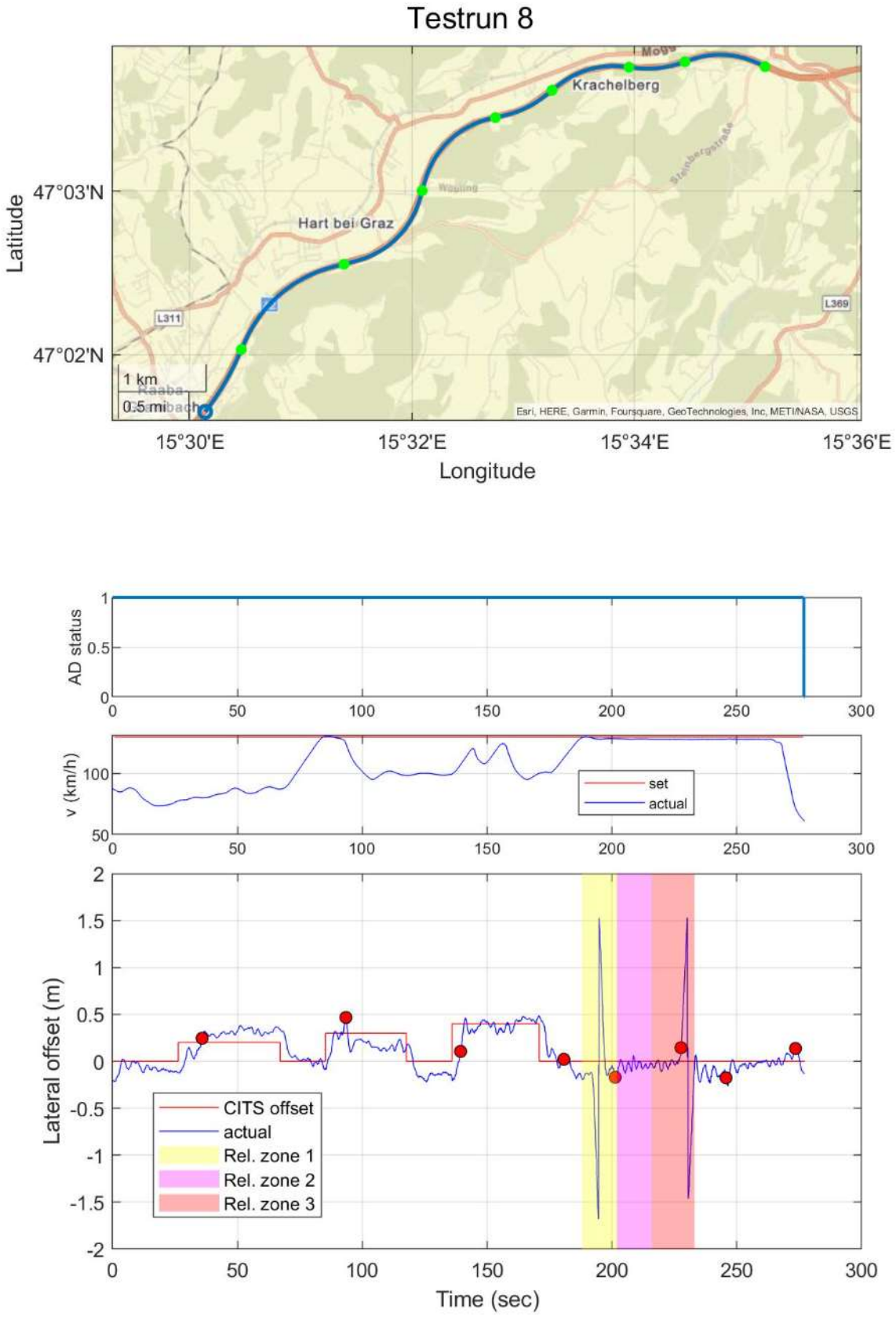

Figure 16: Test run 8 at 130 kph.

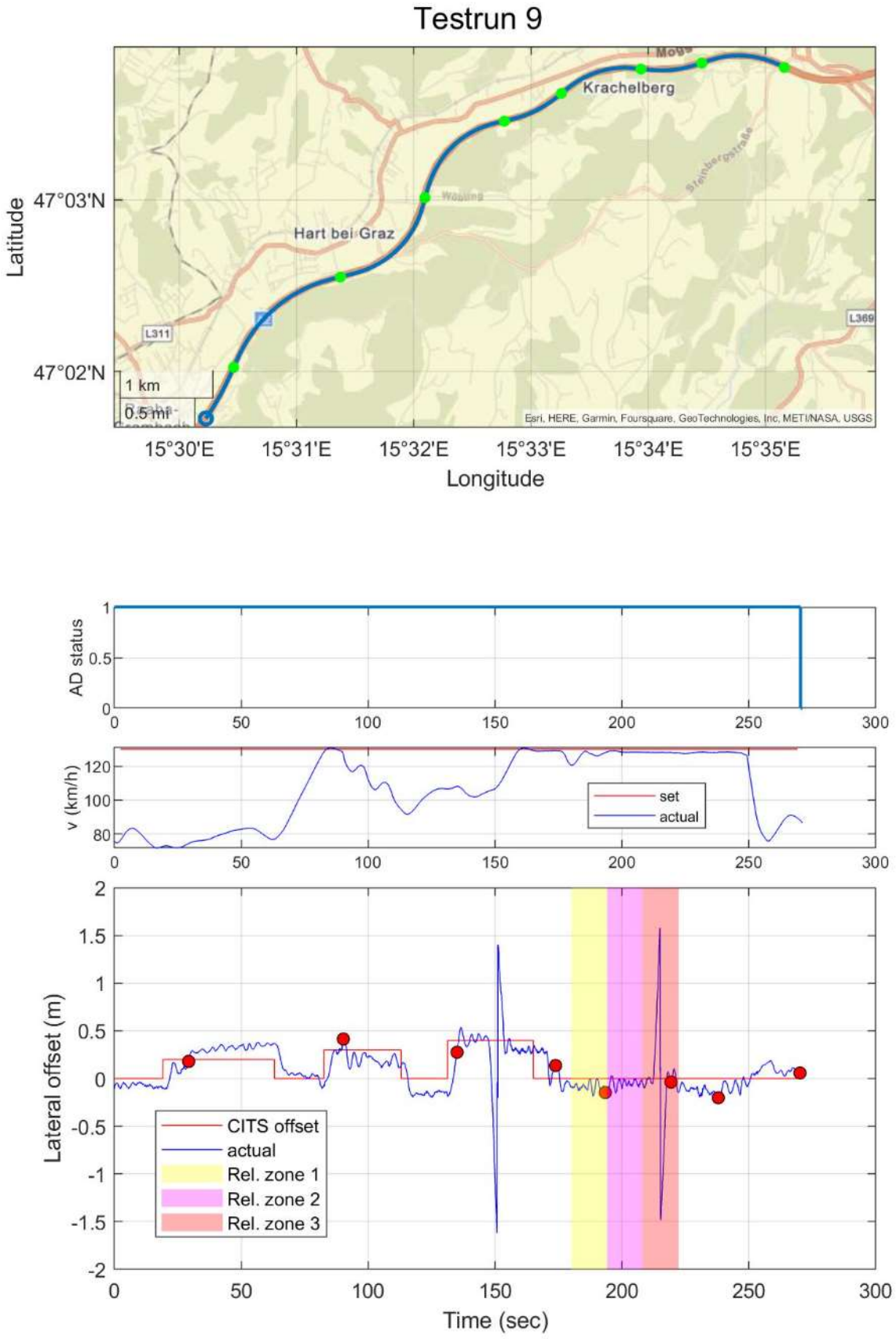

Figure 17: Test run 9 at 130 kph.

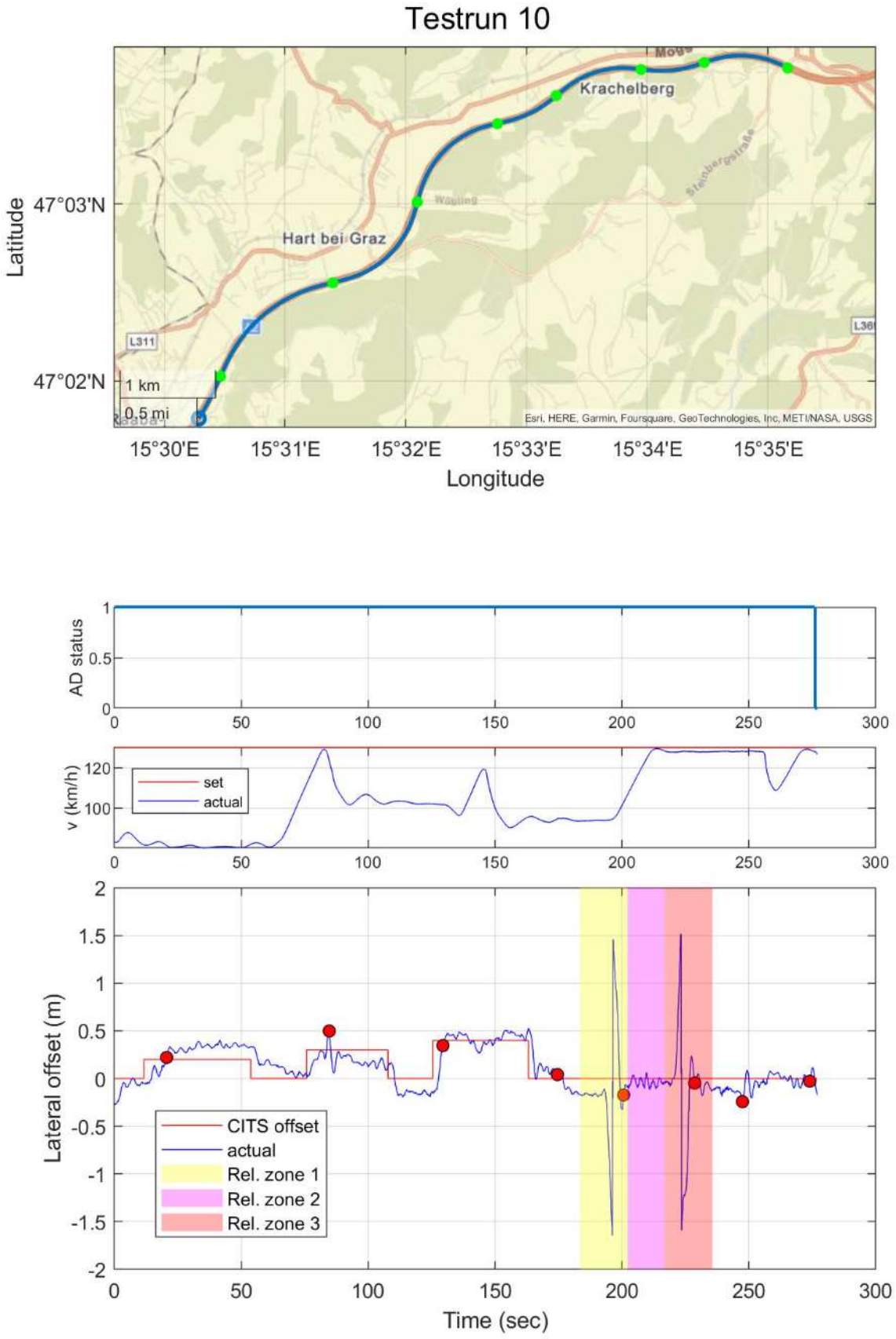

Figure 18: Test run 10 at 130 kph.

2.5. Observations

From the test results, we can see that the lateral offset has some deviation from the desired offset. In between being about constant, the lateral offset changes its magnitude “spontaneously”. These effects were also noticeable during the test drives corresponding to changes in the road slope which in turn correspond to the road curvature.

To highlight this effect, we further analyze the trajectory from test run 3, see Figure 19. A green dot in the geographic plot shows a point on the road of zero curvature, indicating a change of sign in road curvature, i.e., going from a left turn into a right turn or vice versa. The corresponding instances in time are shown by the red dots in the second row w.r.t. the lateral offset. Especially for t > 230 sec, where the desired offset was 0, the correlation of the road curvature and the lateral offset is obvious.

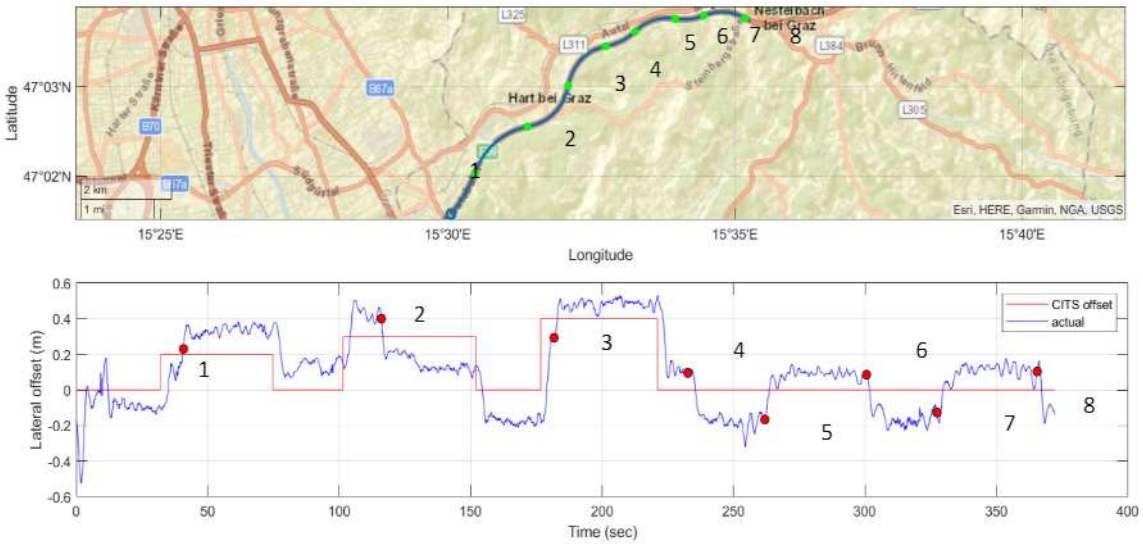

Figure 19: Correspondence of road slope, road curvature and lateral offset.

It is worth noting, that in addition to the road slope, also the look-ahead distance of the steering controller adds to error of the lateral offset but is also a result of the road curvature.

The reaction time to a step in the desired offset is mainly determined by the form of the planning curve. A Polynomial of 5th order is used to build up a continuous transition to the new offset.

We tested on the road steps of 20, 30 and 40cm. Figure 20 shows a step from 20 cm to 0 cm offset. The blue line shows the measured actual offset, the green line the offset determined by the CITS message (IVIM) and the cyan line planned offset. As discussed above the measured offset is biased. To make the timings better visible the yellow line shows the actual offset with correction of the bias due to curvature and other effects.

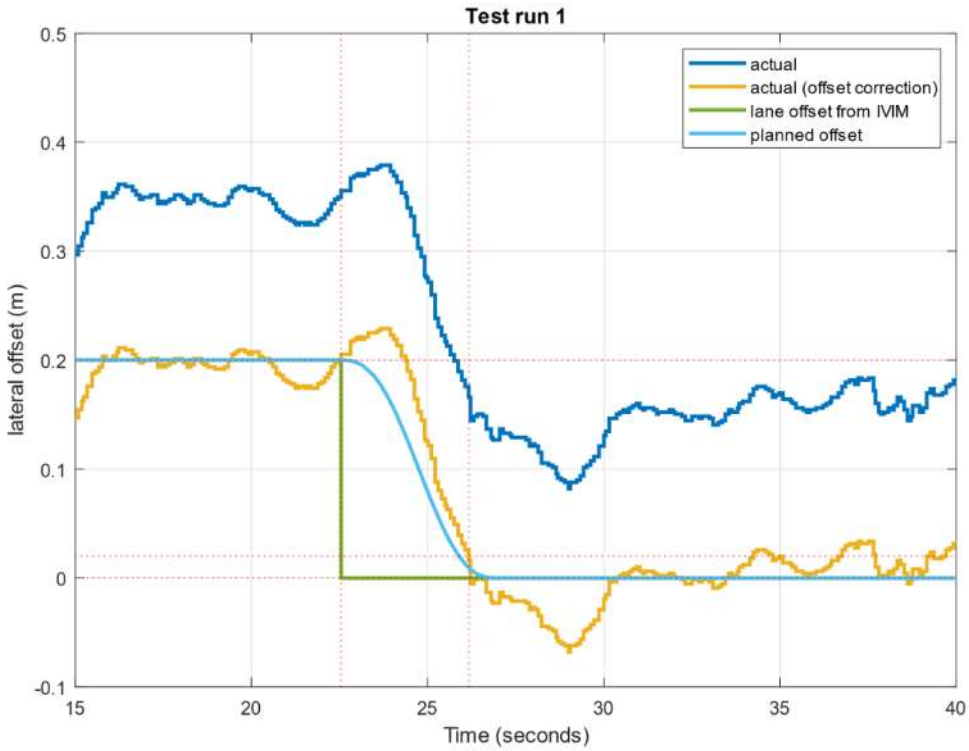

Figure 20: Offset risetime.

As definition of reaction time we use the time form the step in lane offset from IVIM until 90% of the step height is reached.

Offset step	0 to 20cm	20 to 0cm	0 to 30 cm	30 to 0 cm	0 to 40 cm	40 to 0 cm
Test run	reaction time [s]					
1	-	3.6	3.4	3.4	4.5	3.4
3	3.45	3.5	3.1	3.55	2.8	3.3
4	3.3	3.2	2.7	3.5	3.3	-
5	3.4	3.7	3.05	3.4	3.55	4.9
6	3.5	3.6	2.95	4.3	3.4	2.6
7	3.1	2.4	3.1	3.5	5.2	4.6
8	3.4	3.4	3.15	3.95	4.3	3.3
9	3.35	4.5	3.7	3.2	4.2	6.4
10	3.3	3.1	4.9	3.4	4.45	2.3

Table 2: Reaction time to a step in the desired offset.

Table 2 shows the measured reaction times. In two cases no reaction time could be measured. Test run 1, step 0 to 20 cm was not part of the logged data. And in test run 4, step 40 to 0 cm there was an overlay with a lane change and therefore it was not possible to determine the reaction time.

The mean value of all measured reaction times is 3.59 s.

In test run 1 the test vehicle traveled on the rightmost lane until it reached the relevance zone 1 of the IVIM (virtual road damage). There it executed one lane change to the left, avoided the leftmost lane in relevance zone 2 and executed one lane change to the right in the relevance zone 3. The desired speed was initially chosen as 85 kph due to a temporary speed limit and was raised to 90 kph during the test drive. The actual speed was regulated according to the surrounding traffic and stayed, with exception of on short overshoot below the desired speed.

Test run 2 was aborted due to heavy rain, which causes malfunction of the mobile eye camera.

In test run 3 no lane changes were executed.

In test run 4 the test vehicle traveled on the middle lane through the area with the offset recommendation. After this area the vehicle was manually set to manual driving and was driven to the rightmost lane. There automated driving was activated again, and the test vehicle performed lane changes as in test run 1.

In test run 5 the test vehicle executed lane changes as described at test run 1.

In test run 6 the test vehicle drove on the rightmost lane. Due to the traffic, it was not able to execute a lane change as requested by the IVIM. Only at the end of relevance zone 2, traffic allowed performing a lane change, which was finished in relevance zone 3, where the vehicle is allowed to choose its lane freely. After leaving relevance zone 3, the test vehicle executed an automated lane change back to the rightmost lane.

In test run 7 and 8 the test vehicle executed lane changes as described at test run 1.

In test run 9 the test vehicle started on the rightmost lane, due to surrounding traffic it executed a lane change to the middle lane in the third area with offset recommendation (40 cm). In relevance zone 1 the test vehicle was already not on the rightmost lane, which should be avoided according the received IVIM and stayed on the middle lane until the indicated that the rightmost lane was available again in relevance zone 3 by the IVIM.

In test run 10 the test vehicle executed lane changes as described at test run 1.

Test run	Lane change in relevance zone 1	Lane change in relevance zone 3
1	✓	✓
3	x	x
4	✓	✓
5	✓	✓
6	x *	x
7	✓	✓
8	✓	✓**
9	x ***	✓
10	✓	✓
Successful/total	6/9	7/9

Table 3: Test run and lane change execution.

** Traffic prohibited execution of lane change*

*** The lane change was started in relevance zone 3 but ended afterwards. This is no problem, because the automated vehicle is allowed to choose its lane freely in relevance zone 3.*

**** Traffic situation caused the automated vehicle to change to the left lane before entering reference zone 1 and therefor it was no need to change the lane in relevance zone 1.*

2.6. Conclusion

The main findings from the test drive are as follows:

- Both, C-ITS triggered in-lane offset as well as lane changes could be demonstrated successfully.
- In-lane offset
    - Lateral road slope caused the vehicle to deviate from the desired in-lane offset, e.g. Figure 21.
      Therefore, the lateral controller of an automated vehicle making use of C-ITS based lane offsets must be able to compensate lateral deviations caused by road slope, side wind and other disturbances.
    - The in-lane offset of 40 cm was quite close to the vehicles on the nearby lane, especially trucks, reducing the overall driving comfort.
    - In-lane offsets maxing out the current lane width might make it necessary to also apply an in-lane offset on the nearby lane to maintain a safe distance. Otherwise, the measures to avoid the emergence of lane grooves might be very limited.
    - In summary, precise navigation around potholes or lane grooves raises very strict requirements on the tracking accuracy of the vehicle's steering controller.
- Lane changes
    - In contrast to lane-offsets, in general lane changes cannot be performed instantaneous. Sometimes it might be impossible to do the lane change due to dense traffic.

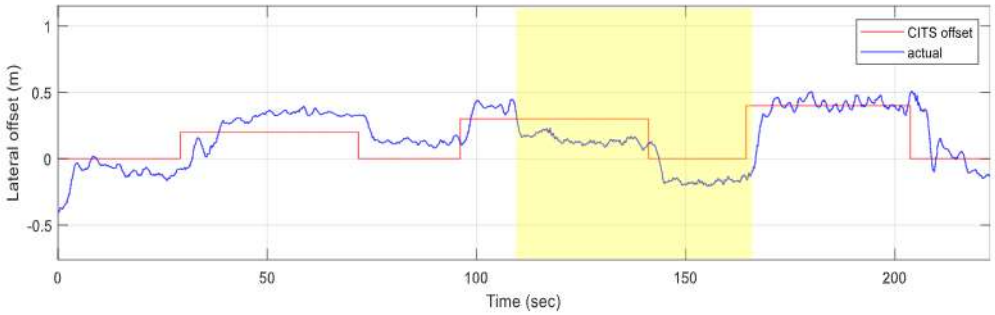

Figure 21: Road slope resulting in a lateral offset (yellow highlighted section).

SECTION 3: BASELINE PERFORMANCE ANALYSIS OF THE END USER LOCALIZATION SYSTEM

In this section we present a summary of the performance of the end-user vehicle localization system as implemented in WP3. The intention is to present to the reader the main characteristics and rationale behind the adopted solution and the associated measured performance. These shall serve to put into context the results presented in later sections as well as the whole text of this deliverable.

The ultimate goal of the end-user localization system for the end-user vehicle is to produce as accurate, precise and secure position estimates as technology can produce nowadays for general automotive applications. The methods and HW were initially decided during the first phase of the project, and have been reported in deliverable D3.1. For the high accuracy and precision required, RTK positioning was selected. Among the existing RTK methods, the use of data/observations from the nearest station was considered the one offering the best performance, and was then selected as the preferred method. This requires the end-user vehicle to be relatively near the reference station (less than 10-20km). In cases when this distance is larger, the use of so-called virtual reference stations (VRSs) was deemed the optimal choice.

The security aspect of the position is to be delivered via the use of Galileo's OSNMA. This service allows receivers to assess the authenticity of the navigation messages transmitted by Galileo

satellites and of the satellites themselves. This information can then be used by the receivers to compute position estimates. It is important to note then, that OSNMA does not provide instructions for the receiver to compute authenticated PVT solutions: how to use this information is decided by the receiver manufacturer. It is clear nevertheless that most secure position that a receiver can provide using only OSNMA is one computed using only navigation messages and signals from OSNMA authenticated satellites. This limitation has two relevant consequences. First; because at the moment OSNMA supports the authentication of only Galileo satellites and their navigation messages, a strict usage of only OSNM authenticated satellites would prevent the use of other constellations, which would restrict the achievable accuracy. And second: OSNMA only makes it possible to detect certain types of spoofing attacks, but not all.

Having these limitations in mind, the goals in ESRIUM in relation to the provisioning of highly accurate and authenticated position were further clarified. The aim then is to emphasize accuracy over authenticity, hoping that in the future OSNMA includes support for the authentication of GPS satellites (as it is expected to happen) and that perhaps further enhancements pertaining security become more widely available. A pertinent question was then what is the performance associated to a strict use of OSNMA (which at the present moment imposes using observables and navigation data only from authenticated Galileo satellites) in comparison to what could be achieved when/if OSNMA supports the authentication of GPS satellites/navigation messages. The characterization of the end-user vehicle localization system has then been done trying to assess this potential performance gain, and tests were done in different environments in Finland and Austria to evaluate the impact of this and other relevant factors such as the type of scenario and overall setup. Similar considerations apply to other results presented in this deliverable, where the impact of using OSNMA in a strict sense will be evaluated.

3.1. Experiments in Finland

The results from the experiments carried out in Finland to characterize the end-user localization module were reported in detail in Deliverable D3.3. In this document we now present a short summary of the main results relevant to the content of the present document.

In order to devise results that could be extrapolated to typical modern receivers used in automotive applications, the receivers used in the tests (Mosaic X5 from Septentrio) were configured to use observables from the GPS L1/L2 and Galileo E1/E5a bands (dual band) to produce RTK positions when possible and standalone ones otherwise. Thus, the receivers produced three types of solutions:

- RTK-fixed, when the receiver could solve the cycle ambiguities of the carrier phase (that is, when it could estimate the number of entire wavelengths of the carrier wave from the satellite to the receiver).
- RTK-float, when RTK positioning was possible, but the receiver could not compute the cycle ambiguities.
- Standalone, when the receiver could not use RTK.

Being RTK a differential positioning method, it requires the availability of different types of information from a reference station, information that is made available by a positioning service provider. In Finland, the provider was FINPOS, the state-owned and maintained positioning service exploiting the (also state owned and maintained) FinnRef network of reference stations. The information from the reference station (e.g. observables, its position and the coordinate reference frame of this position) was sent to the receiver in the end-user vehicle via RTCM messages, which is a communication standard devised to send GNSS related information via Internet.

Among the different RTK positioning techniques, the use of the nearest reference station was selected. For this purpose, FINPOS makes available a service by means of which, upon receiving an approximate position of the receiver, it automatically selects the closest reference station and sends to the receiver its corresponding RTCM messages.

In relation to OSNMA, each receiver was configured to use a different OSNMA configuration:

- One using OSNMA in strict sense (denoted as "OSNMA-strict" in the rest of the document). As explained before, this configuration precluded the use of non-Galileo signals.
- One not using OSNMA (denoted as "OSNMA off" in the rest of this document) and therefore using all the mentioned signals from the two constellations.

The intention behind using these configurations is to the performance in terms of accuracy and availability that can be achieved as of now using OSNMA for authentication to the one that could have been achieved had OSNMA supported also the authentication of GPS satellites and navigation messages.

The tests were done in highways (mostly open sky scenario) and urban ones with different degrees of signal obstruction. As expected, the use of OSNMA in strict sense and the obstruction degree were observed to be factors greatly impacting the overall performance. This can be seen in Figure 22, which presents the proportion of solution types attained. The figure clearly shows that using OSNMA in strict mode and the presence in an obstructed environment strongly decrease the proportion of RTK-fix solutions attained, which are the most accurate ones. Table 4 and Table 5 present the corresponding overall 95% horizontal accuracies (that is, the 95% percentile of the horizontal errors) and the availability of position estimates with less than 10 cm of horizontal error, where the results are computed including the three position types attained. In the best case (open sky with OSNMA off) the receiver could compute positions with a horizontal error below 14 cm 95% of the epochs where a position was available, and positions with less than 10 cm of horizontal error during 92.42% of the time. In contraposition, in the worst case (in urban scenario and with OSNMA on) the horizontal error was under 18.47 m in 95% of the cases when the receiver could compute a solution, and solutions with horizontal errors smaller than 10 cm were available less than 5% of the time. As can be seen in Figure 22, this case was characterized by the absence of RTK-fix positions, and by a majority of epochs in which positioning was not possible at all.

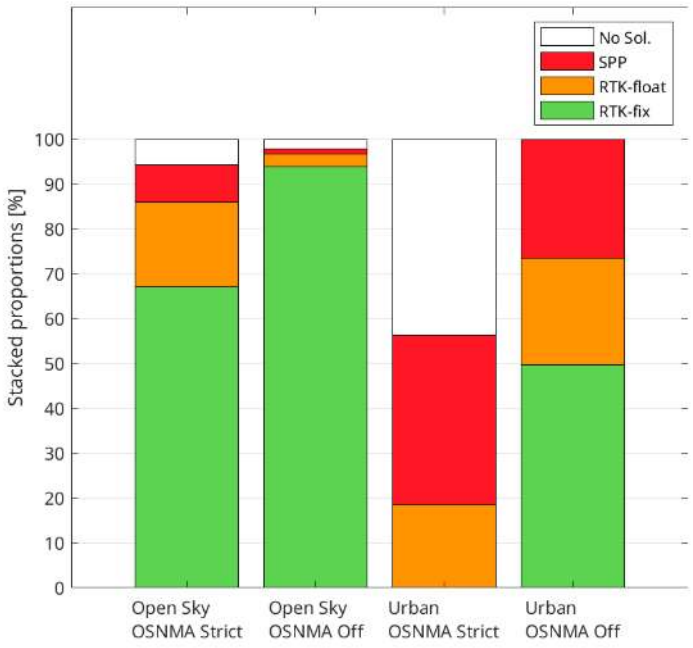

Figure 22: Proportion of solutions attained in the test carried out in Helsinki.

Figure 23: Trajectory followed in Helsinki downtown an attained solution types with OSNMA in off (left) and strict (right) modes, respectively.

OSNMA / Env.	OFF	Strict
Open Sky	0.14 m	0.75 m
Urban	10.19 m	18.47 m

Table 4: 95% percentile of the overall horizontal positioning errors during Finland tests.

OSNMA / Env.	OFF	Strict
Open Sky	92.42%	74.10%
Urban	39.63%	4.68%

Table 5: Availability of position estimates with horizontal error < 10 cm during the Finland tests.

3.2. Experiments in Austria

Similar types of experiments were carried out in Austria, in particular using the same receiver, signals and positioning mode (RTK with fallback to standalone). In addition, the tests were also carried in several types of environments with different degree of obstructions ranging from open sky (a highway) to urban downtown. Nevertheless, there were some relevant differences that can affect the overall performance and therefore are note-worthy:

- The positioning service provider was EPOSA, a nation-wide commercial service provider in Austria, and a virtual reference station (VRS) was used. This means that the information from the reference station used by the receiver correspond to a non-existing one (and therefore called "virtual") located in a position near the end-user vehicle during the experiments. The use of this technique can result in appreciable performance differences with respect to using the nearest reference station (NRS), especially in cases where the density of stations of the reference network is relatively small.
- The tests in Finland were carried out at relatively high latitudes, where a receiver is likely to observe more satellites located in the South than in the North. In Austria this effect is less probable.
- In addition, other geometrical and atmosphere-related differences attributable to being in different locations and time.

These differences and their possible impact then justify the need to make performance assessments in significantly different areas (southern Finland and Austria) and at different times.

As explained before, OSNMA provides authenticity related information, and does not provide instructions about how to compute PVT solutions using this information. It is then up to the receivers how to use this information. As we have also explained, aiming for OSNMA-authenticated PVT solutions in a strict sense (where only authenticated Galileo satellites are used) results in a significant performance loss due to not using satellites from constellations other than Galileo, from which the receiver does not have any authenticity-related information. To alleviate this limitation, receiver manufacturers are devising modes to compute PVT positions using OSNMA in a less stringent manner. One such strategy is to use all the satellites from which the receiver has a) either a positive

authentication (as provided by OSNMA), or b) no authenticity-related information. Such strategy is implemented in the receivers used in our tests, and the manufacturer calls it "loose". Henceforth, we will use the term "OSNMA-loose", or OSNMA in loose mode, to refer to this positioning strategy and/or its associated results.

The use of OSNMA in loose mode in our tests implies that the receiver could use a) authenticated Galileo satellites and b) all GPS satellites. This still represents a smaller number of satellites with respect to using all available ones from Galileo and GPS, and therefore a slightly worse performance is expected. This small performance degradation is not so much due to the occurrence of real spoofing attacks, but to the use of cross-authentication in Galileo. In essence, cross-authentication allows the authentication of a satellite and its navigation message using OSNMA data sent by a different satellite. This is used in OSNMA for the authentication of Galileo satellites themselves, where only a portion of satellites transmit OSNMA data, and the authentication of the rest can be done using cross-authentication. The consequence is that, when a satellite that is transmitting OSNMA data is not visible, the receiver will avoid the use of that satellite plus others that would need the OSNMA data from this satellite for their (cross-) authentication. This issue and its potential impact have been studied in detail in ESRUM, and reported in Deliverable D3.3.

We now proceed to show an example of the observed performance. A more in-depth analysis will be presented in a forthcoming scientific publication. The results presented here are based on the analysis of the data collected during one continuous driving session lasting approximately three hours. During this session the car traversed areas with different obstruction degree. Those were manually classified as open sky (e.g. a highway and rural areas) and urban (essentially inside Graz city).

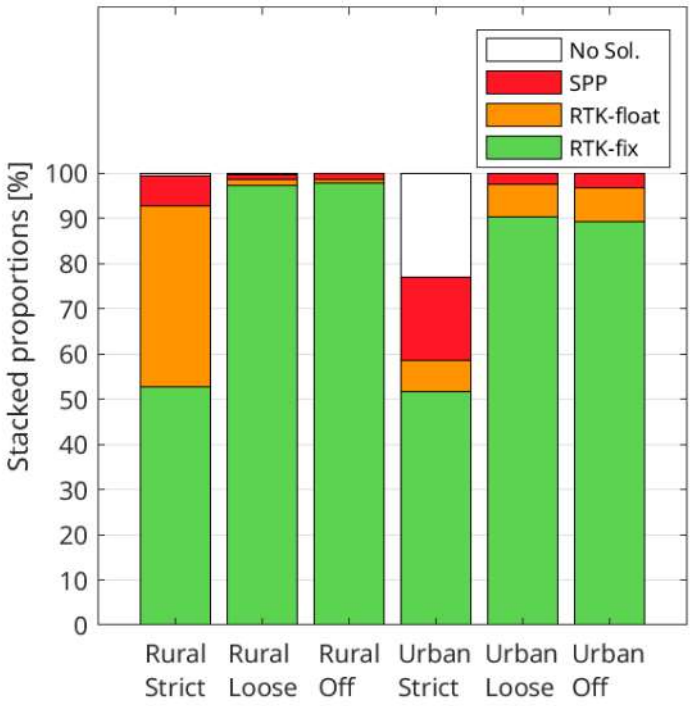

Figure 24: Proportions of attained solution types in the different environments and with the three OSNMA configurations.

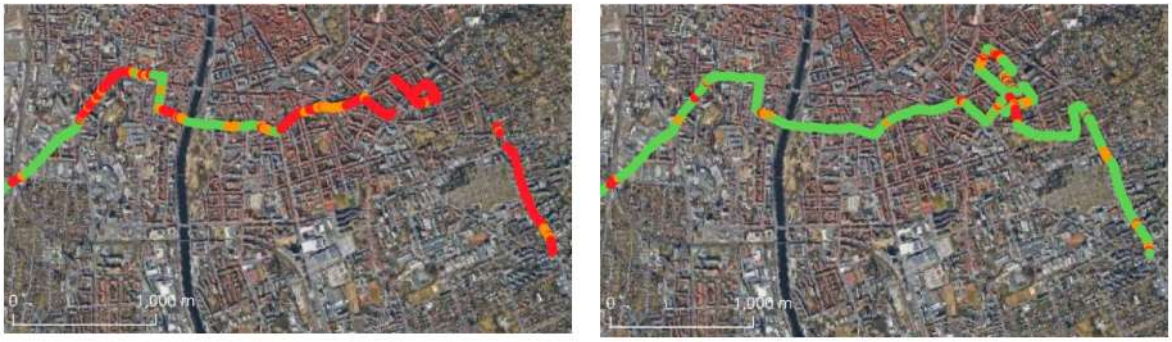

Figure 25: Trajectory followed in Graz downtown an attained solution types with OSNMA in off (left) and strict (right) modes, respectively.

OSNMA / Env.	OFF	Strict
Open Sky	0.04 m	1.30 m
Urban	0.39 m	11.16 m

Table 6: 95% percentile of the horizontal errors attained during the tests in Austria.

Env.	OFF	Strict
Open Sky	97.79%	51.70%
Urban	90.09%	53.27%

Table 7: Availability of positions with a horizontal error less than 10 cm during the test in Austria.

Figure 24 shows the proportion of position types attained in the open sky and urban environments by the three receivers using different OSNMA configurations. From the figure one can immediately see that, as expected, the proportion of RTK solutions significantly decreased when OSNMA is used in strict mode with respect to not using OSNMA (in off mode), whereas its use in loose mode did not have a meaningful impact. The impact of the OSNMA mode along the trajectory followed in Graz downtown can be seen in Figure 25. The overall horizontal accuracy computed over all position types can be seen in Table 6, where we see that the 95% error percentiles significantly increase when OSNMA is used in strict mode (from 4 cm to 1.3 m in open sky, and from 39 cm to 11.16 m in urban). Table 7 shows the consequent reduction of the horizontal availability, where we see that positions with horizontal errors smaller than 10 cm in open sky were attained 97.79% of the time when OSNMA was not used versus 51.70% when in strict mode. Similarly, a reduction from 90.09% to 53.27% was observed in the urban environment.

Comparing these results with those obtained from the tests in Finland, it is worth noting that the overall accuracy was higher in Austria, where in the best case (open sky with no OSNMA) was of 4 vs. 14 cm in Finland. The horizontal availability followed accordingly, being 97,79% and 92.42% in Austria and Finland, respectively. This difference could be the consequence of the differences between the positioning service provider used, the RTK mode (NRS in Finland and VRS in Austria) and the overall constellation geometry, as explained in the beginning of this section.

3.3. Conclusions

The performance of the end-user vehicle positioning system depends not only on the quality and capability of the selected receiver, but also on "outer" factors that do not directly pertain its design. Some of these are predictable and controllable to some extent, such as the selection of the positioning service provider, whereas others are not, such as the characteristics of the environment, the overall satellite geometry, and the atmospheric conditions (ionosphere and troposphere). The results from the tests carried out in Finland and Austria can be taken as an example of a realistic range of performance that one can expect in countries with good quality positioning services available.

The accuracy is an important performance indicator, especially the horizontal one for automotive applications. However, more important is the availability, which takes into account the possible lack

of PVT computations in some epochs and better represents the overall quality of service that can be expected in a real scenario. Accuracy and availability are then to be interpreted together. The main target scenario type in ESRIUM is highway, which can arguably and typically be qualified as open sky. For this type of scenarios, the results from our tests suggest ranges of attainable horizontal accuracy (in terms of the 95% percentile) between 4 cm to 14 cm when OSNMA is off and using only Galileo and GPS satellites in RTK positioning, and corresponding availabilities of between 92.42% to 97.99%. This level of service can be considered as compliant with the requirements formulated in the ESRIUM project (0.3 m of lateral deviation 95% percentile, see Deliverable D2.1).

In relation to the need to provide authenticated PVT solutions, the results from the tests in Finland and Austria confirm the existence of a significant trade-off between availability of accuracy and authenticity. The cause of this trade-off is the fact that OSNMA only supports the authentication of Galileo satellites. This significantly restricts the satellite availability, which in turn reduces the accuracy and can make the computation of positions (especially RTK) impossible in obstructed environments such as urban scenarios. In highways, the target scenario in ESRIUM, the range of attained overall accuracy were of between 0.75 m and 1.3 m. This would result in non-compliance with respect to the accuracy requirements. Because of this trade-off, OSNMA is to be used in loose mode, which leverages a well-balanced mixture between accuracy and authenticity as per the project goals. In our tests in Austria, this performance has been shown to be similar in practice to that attained with OSNMA off. Nevertheless, one should be cautious when extrapolating this performance to other scenarios.

The overall impact of OSNMA in the positioning performance justifies the study of its impact on other applications that rely on the provision of high accuracy, such as trajectory following.

SECTION 4: ANALYSIS OF THE TRAJECTORY FOLLOWING USE CASE

In this use case, we present a comparative analysis of EGNSS-based path tracking with and without open service navigation message authentication (OSNMA). The EGNSS receivers provide dual-band GPS L1/L2 and Galileo E1/E5a RTK positioning for cm-level GNSS localization. The path following task utilizes the accurate RTK-assisted EGNSS position and heading information to track a reference path. The lateral error from the reference path is used as the correction signal for the tracking controller. We compared the performance of the tracking controller in an open-sky and urban setting within the Graz University of Technology campus using an automated driving demonstrator vehicle. The positioning utilized two different OSNMA schemes, namely ``strict'' OSNMA solution that utilize only authenticated Galileo satellites or not using authentication, implying utilization of all the available GNSS satellites.

To analyze the effect of OSNMA authentication on positioning accuracy, a path-tracking use case was performed with and without OSNMA authentications. The specific use case we implemented is illustrated in Figure 26, where the reference path is provided to the vehicle beforehand. This implementation was then used in two different test cases, namely in an open-sky and urban location, with two different OSNMA settings to analyze its effect on the automated driving performance.

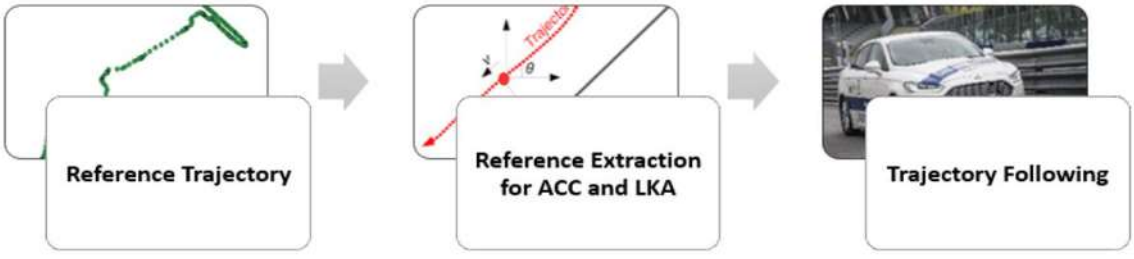

Figure 26: Path following use case.

The test vehicle setup is described in Deliverable 5.1. To implement fully automated GNSS-based tracking of a given reference path, the driving function is composed of the following components:

- A path follower function which finds the section of the reference path related to the current position of the vehicle.
- A speed control function, which calculates a desired acceleration based on the deviation from the set speed and speed constraints due to the curvature of the path section from 1.
- A lateral controller, which calculates the path tracking error and from that, the desired steering wheel angle.
- A longitudinal controller actuating the brake/throttle commands to regulate the vehicle's speed.

The reference path was obtained in the following way:

1) A manually driven trajectory was logged with a high-precision GNSS system.
2) The section of interest was extracted from the logged data resulting in a list of waypoints.
3) The final reference path was then obtained from a spline approximation algorithm.

The boundary conditions for the spline approximation were set so that the resulting reference path is a closed path which allowed to do several consecutive rounds of uninterrupted autonomous driving. This is important to obtain "steady state" path tracking results, as there was no measure implemented which guarantees the same initial conditions of the individual test runs.

In this way, the reference path for open-sky (Figure 27) and urban scenario (Figure 28) was obtained.

Figure 27: Reference path for the open-sky scenario.

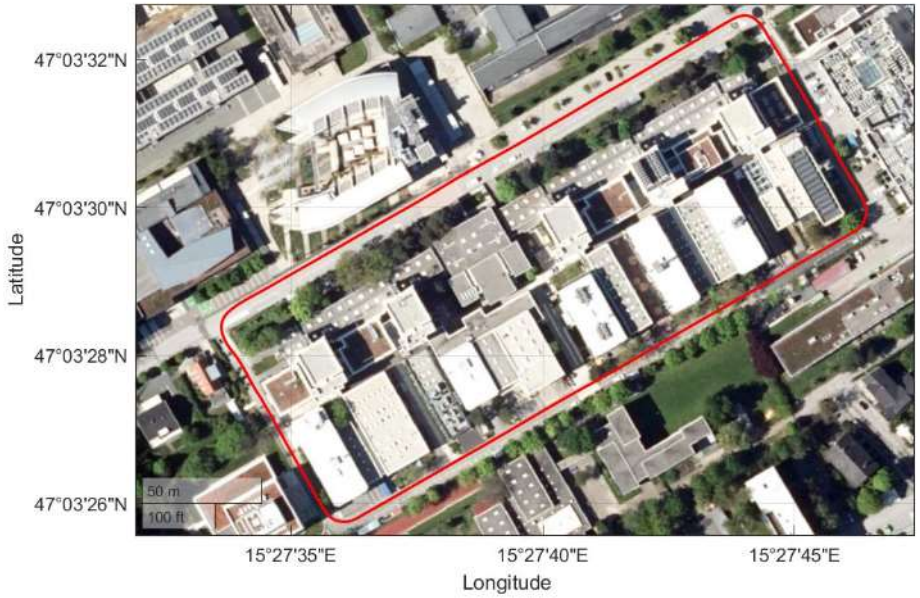

Figure 28: Reference path for the urban scenario.

4.1. Results

Figure 29 shows the path following results under open-sky with OSNMA disabled (blue) and OSNMA enabled (red). The first sub-figure on the top shows the reference path and the logged vehicle position. The sub-figures below show the steering wheel angle, look-ahead distance, lateral error, and vehicle speed v in order from top to bottom. Four rounds of the circuit have been performed each for OSNMA-disabled and OSNMA-enabled settings.

Especially the straight sections of the reference path indicate, that the OSNMA feature does not influence the positioning accuracy

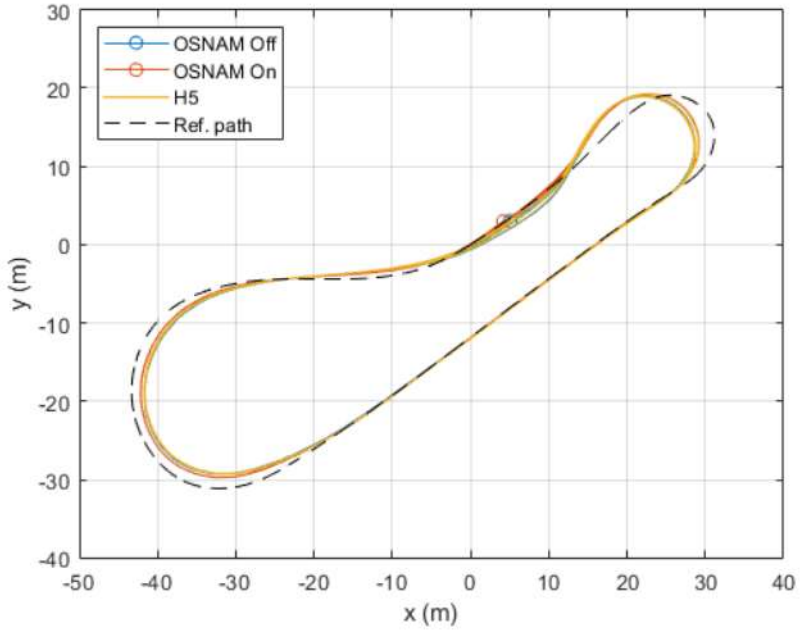

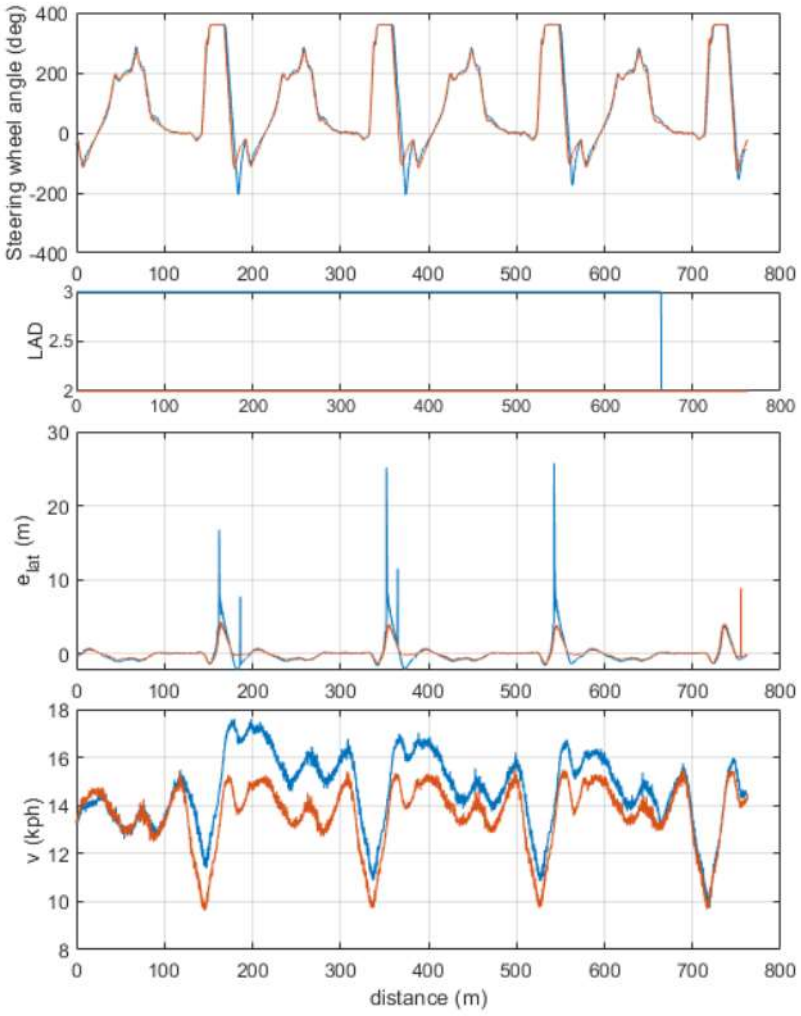

Figure 29: Results of the open-sky scenario

For the urban driving test case, a large loop within the Graz University of Technology was used. There are dense buildings and trees along this track to cause sufficiently high interference and multi-path reflections to degrade the GNSS location solution. During these experiments, OSNMA-on (which is only using enabled Galileo Satellites) setting provided no RTK-assisted solution. Therefore, stable tracking was not possible due to positioning errors resulting from multi-path signals and the lack of sufficient visible satellites supporting OSNMA. In this case, path following only without OSNMA was tested. Even with OSNMA turned off, multi-path signals can cause deviations in sub-meter ranges, which affects GNSS-based tracking performance.

The general observation was that path following works but is not reliable due to the changing RTK localization types due to multi-path signals, indicating changeable or unstable positioning accuracy, thus resulting in wavy and unreliable tracking behavior.

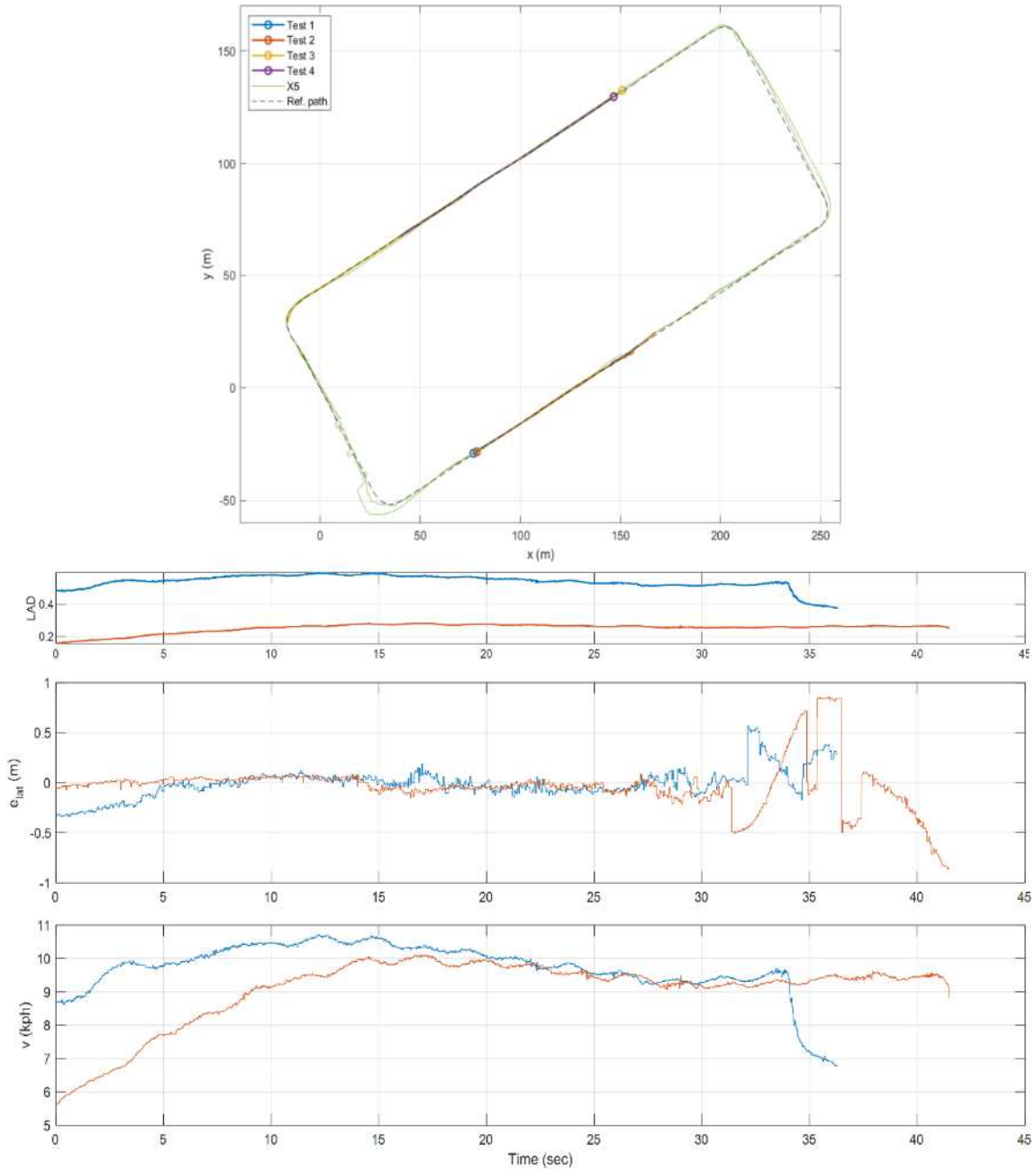

Figure 30: Results of the urban scenario.

4.2. Conclusion

The experiments indicated that the use of OSNMA under open-sky conditions is feasible with limitations. Even with OSNMA turned off, sub-meter deviations can lead to control performance issues of the automated vehicle. This can be attributed to the very low number of OSNMA-enabled EGNSS satellites as well as the instantaneous changeability of the RTK solution method.

Particularly for urban settings, multi-path effects can lead to severe degradation in localization solutions, which exacerbates accuracy and tracking performance. In our experiments, the OSNMA strict setting was unusable in urban settings for accurate or improved localization and OSNMA-off was marginally usable but not acceptable for stable path tracking purposes.

SECTION 5: ANALYSIS OF C-ITS COMMUNICATIONS FOR ROUTING RECOMMENDATIONS AND LOCALIZATION

5.1. Implementation of C-ITS communication

The C-IT communication platform will be given in this section, along with some data analysis of C-ITS communications. The OBU-Interfaces and Vehicle Interaction are shown in the following picture. Vehicle CAPTAIN, also known as "Vehicle Communication Platform to Anything," is the test vehicle's OBU that was created internally by ViF.

Real-Time Multisensor Applications is the abbreviation for RTMaps. A software tool for component-based creation and execution is called RTMaps. The interface between the OBU, EGNSS, and MicroAutoBox II (MABx-II) in ESRIUM is RTMaps. The communication was supported by the implementation of an EGNSS Reader and a Python Bridge.

The connection between the connected automated vehicle and its surrounding infrastructure is made possible via the Python Bridge. When there is a match, it initiates actions by evaluating V2X data with exact position and movement of the vehicle. Real-time processing and the built sophisticated algorithms enable safer, more effective driving as well as enhanced communication.

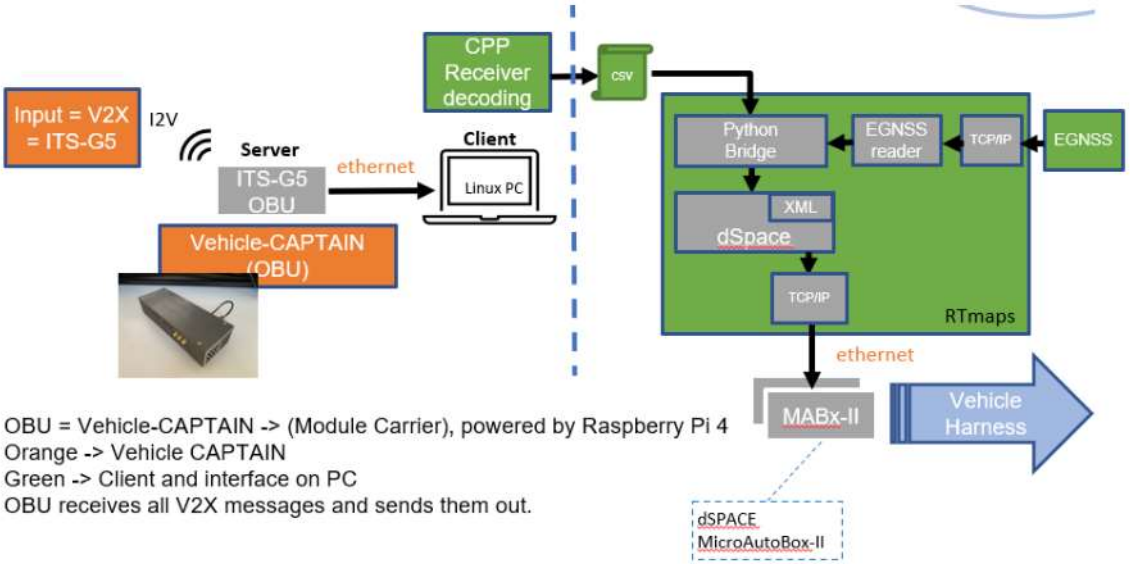

Figure 31: OBU-interfaces and vehicle interaction.

The procedure of validating the C-ITS message (Figure 32) is shown as follows:

- By typing the command, followed by the OBU device's appropriate IP address and port, you may launch the validation application in Docker: ./cppReceiver with the port number 5556 at 172.20.x.x
- The application automatically begins a loop after starting up in which it verifies each message it gets. It specifies the type of V2X message on the screen if it is a V2X message.

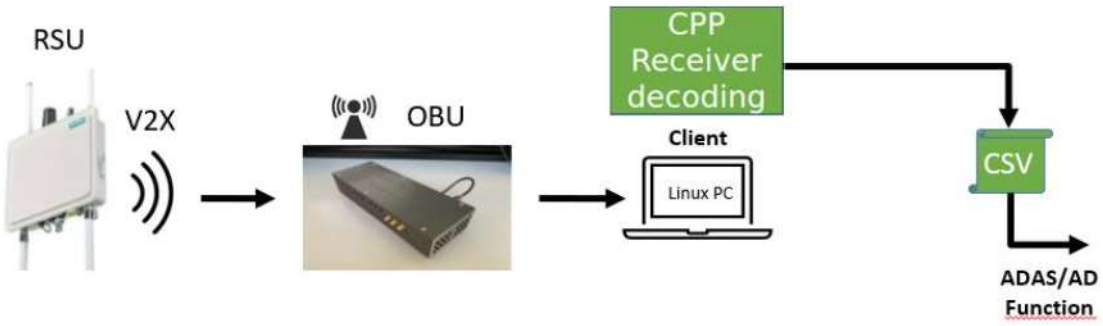

Figure 32: C-ITS message validation.

Using aforementioned hardware and software architecture, VIF collected delay data on the test route from Graz to Laßnitzhöhe. The following analysis of IVI Message Delay is based on our recorded data. We can conclude that there are delays concerning In-Vehicle Infotainment (IVI) messages. Attached are plots with timestamps that illustrate the exact rate of messages received per second by our devices. The first two blue plots represent data recorded with our Vehicle Captain device during two separate drives. On both plots, we can observe similar patterns, with the number of received messages increasing approximately every ten seconds. However, there is noticeable latency, as indicated by a 6-second delay (see Figure 33) in the first drive and a 5-second(see Figure 34) delay in the second drive.

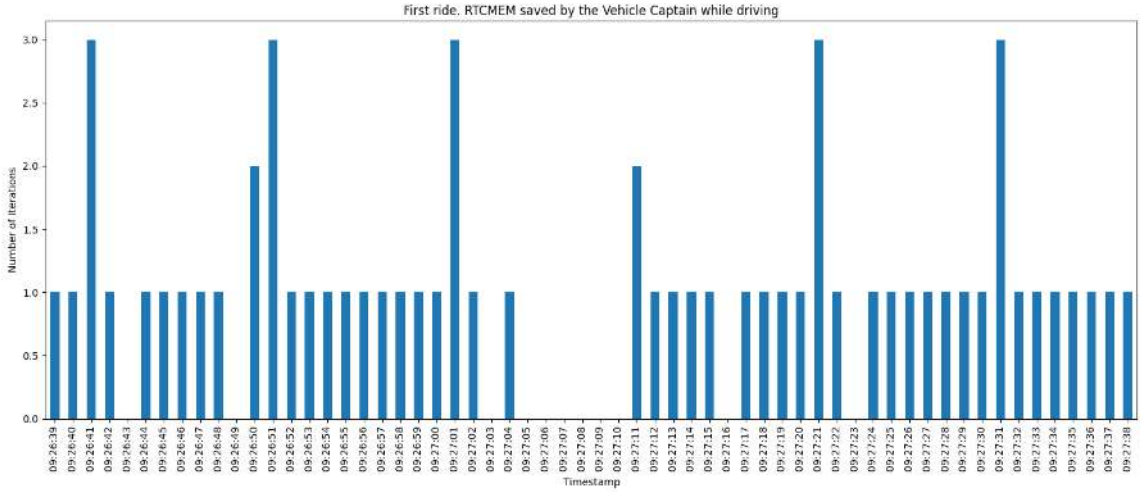

Figure 33: First ride: RTCMEM saved by the Vehicle Captain while driving.

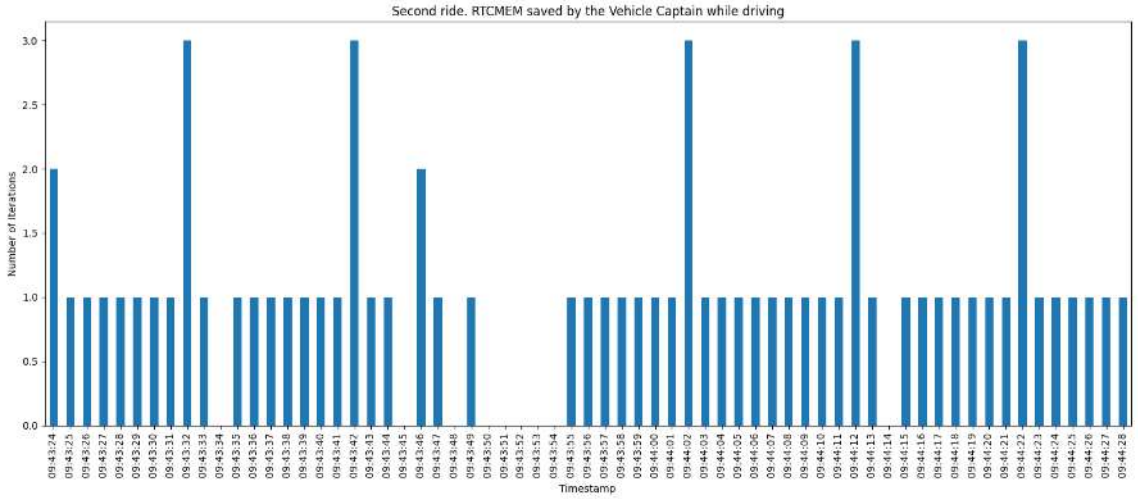

Figure 34: Second ride: RTCMEM saved by the Vehicle Captain while driving.

The second set of plots, displayed in green, presents data recorded with our Cohda Wireless MK5 OBU, taken at a parking area adjacent to the highway. This 7-minute recording exhibits a pattern like the previous plots. Again, we see an increase in the number of received messages every ten seconds. Notably, during periods with no incoming signals for several seconds, we observe spikes in the received message count, sometimes reaching up to 10 messages per second.

5.2. C-ITS communication for RTCM delivery to the GNSS receiver

In order to reach the positioning accuracy and reliability necessary in automated driving, different sensor technologies are typically used. In this context, Real-Time Kinematic (RTK), Global Navigation Satellite System (GNSS) can provide a valuable global position with an accuracy that can reach the cm-level. RTK positioning requires the rover to use different types of measurements and information (typically denoted as corrections) from a positioning service provider, and typically these corrections are sent via Internet/fourth-generation (4G) in the Radio Technical Commission for Maritime Services (RTCM) format. This implies that RTK is not available in regions and areas where 4G is not well deployed.

In addition to benefits in terms of increasing safety, efficiency, and other metrics, the strong expected deployment of Cooperative Intelligent Transport Systems and Services (C-ITS) infrastructure makes it an attractive way for RTCM correction data delivery, which could be used as an alternative or supplement to 4G to expand the RTK coverage. This would significantly increase the availability of high-accuracy localization.

Figure 35 shows a simplified scheme of the main entities that took part in the localization process in our experiments and the flow of information. The equipment installed in the vehicle is represented inside a light-orange square on the right-hand side of the figure. Two Septentrio Mosaic X5 GNSS receivers were connected to the same NavXperience 3G+C geodetic antenna via an active splitter (combination of amplifier and splitter to compensate for the signal power loss due to the signal splitting) and configured to compute RTK positions from GPS L1/L2 and Galileo E1/E5a satellite signals with fallback to so-called single point positioning (SPP) at 20 Hz. Thus, the receivers produced so-called fixed or floating positions when RTK was possible depending on whether they could or not solve for the cycle ambiguities, and SPP when not, where only data from the satellites were used in the position, velocity and time (PVT) computation. Each receiver independently computed RTK positions using the RTCM messages that they received. The upper one received the messages via 4G, and the lower one via C-ITS. The position solutions from both receivers were stored together with additional relevant information for offline analysis.

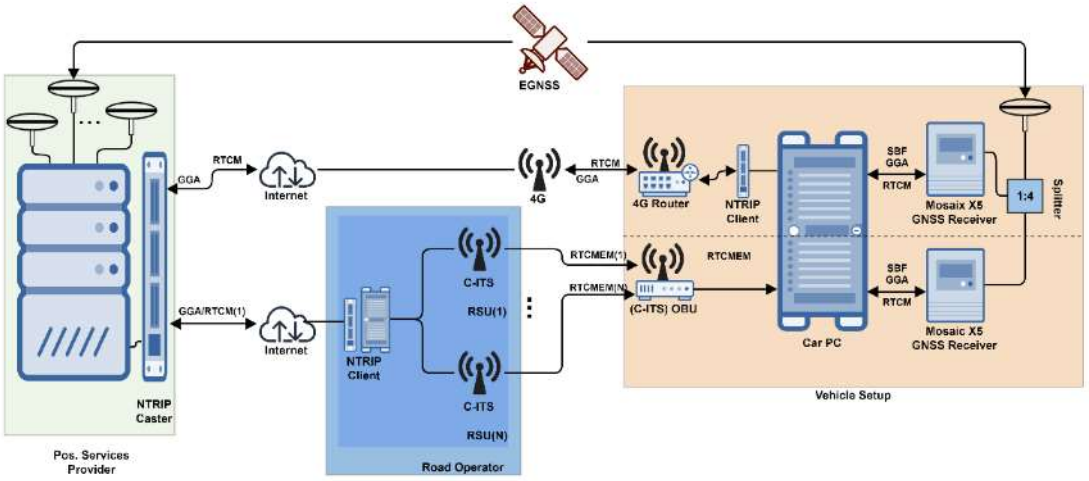

Figure 35: Schematic representation of the information flow.

The RTCM messages were generated by the positioning service provider EPOSA (www.eposa.at) using the virtual reference station (VRS) method. When 4G was used, the GNSS receiver shared its approximate position with EPOSA using the networked transport of RTCM via Internet protocol (NTRIP). EPOSA then generated RTCM messages with observations corresponding to a hypothetical, not existing (and therefore virtual) receiver located near the user's receiver and sent these messages back to the user's receiver. When C-ITS was used to deliver the RTCM messages, an NTRIP client forwarded a mean position of the testing area to EPOSA's NTRIP caster. EPOSA again generated and sent dedicated RTCM messages for the project area to the NTRIP client. The received RTCM messages were forwarded to the road side units (RSUs) used. Once in the RSUs, the messages were encapsulated in RTCM extended messages (RTCMEMs) as per the C-ITS standard[1] and broadcast, received by the on-board-unit (OBU) of cars in the vicinity of the RSUs and then forwarded to the car personal computer (PC), where they were finally converted back to RTCM and handed over to the GNSS receiver.

For our test drive, the Austrian road operator Asfinag prepared two RSUs from Yunex Traffic for RTCM message delivery installed in two gantries separated 900m along the Austrian motorway A2 in the region between Graz and Laßnitzhöhe (cf. Figure 36). The motorway in the testing area has noise barriers on both road margins and the median, as well as hills and trees behind the noise barriers leading to an elevation mask between 15° and 30°.

[1] ETSI TS 103 301 V1.3.1. https://www.etsi.org/deliver/etsi_ts/103300_103399/103301/01.03.01_60/ts_103301v010301p.pdf (2020)

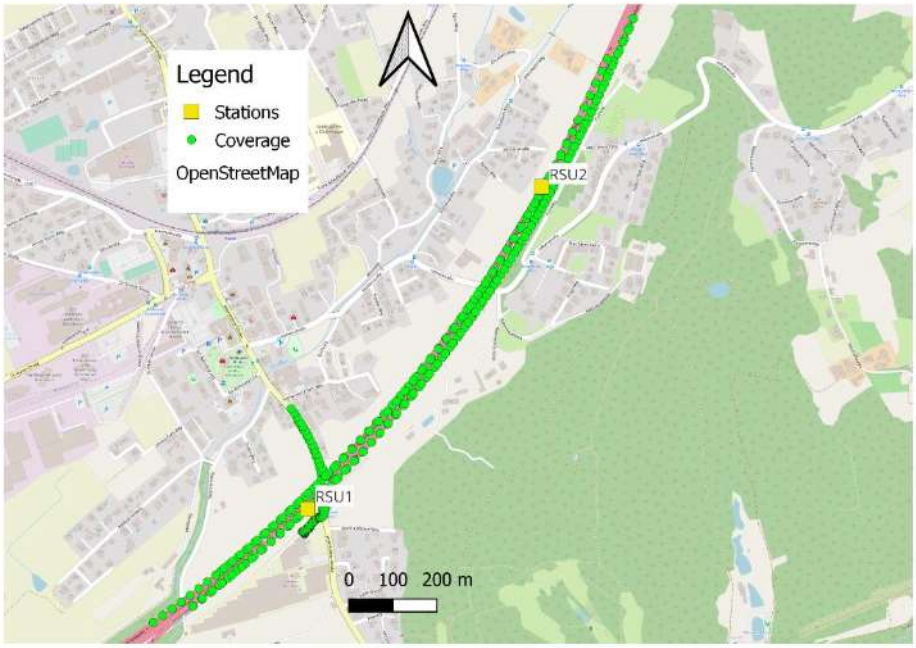

Figure 36: Map of the test region and C-ITS coverage.

RTCM Coverage

Figure 36 shows a map of the test region with the two C-ITS RSU and the coverage of the two RSUs. RSU 1 was installed on a gantry in the northeast direction, and RSU 2 was installed on a gantry in the southwest direction. The green dots show where at the motorway the correction data was received at the GNSS receiver. The test comprises one static period and 4 passes along the motorway, two were driven in the direction of northeast and two in the direction of southwest. During passes 1 and 3 (north-east direction) nearly the same coverage was observed. The first RTCM message was received at a distance of 380 m for pass 1 (390 m for pass 3) from RSU 1. The last RTK correction data was received at 405 m after RSU 2 for pass 1 (430 m for pass 3). Passes 2 and 4 show quite a different coverage. During pass 2, the first RTCM message was received at a distance of 215 m from RSU 2 while during pass 4, it happened in a distance of 370 m. During pass 2, the last RTK correction data was received 240 m after RSU 1, while during pass 4, the last reception was 430 m after RSU 1. In summary, passes 1, 3, and 4 are comparable, while pass 2 shows a worse performance.

To our knowledge, currently, the manufacturer has to guarantee a minimum radius range of 500 m, which would mean that a single RSU has to cover at least 1 km of the road. Furthermore, an expected radius for an RSU should be between 1 and 1.5 km. These numbers could not be reached with our test setup. The maximum distance was about 430 m. During the official inspection and approval, much better performance was documented with distances up to 890 m. Hence, the test setup seems to have some limitations, which are not critical for the demonstration of the use-case of RTCM message delivery for cm-level localization.

RTCM data latency

To analyse the overall latency of the RTCM messages, the mean correction age reported by the Septentrio Mosaic X5 was used, which is the time difference between the GNSS measurement at the GNSS service provider EPOSA till the reception of the RTCM messages at the GNSS receiver.

When comparing the RTCM message delivery via 4G and C-ITS (see Figure 37), the mean message age for the C-ITS-based delivery method was around one second larger on average. The minimum observed RTCM data age of both methods was 0.55 sec. For 4G, the typical age was 0.55 sec rising

up to 1.5 seconds until the next RTCM message arrives (RTCM message rate is 1 Hz). For C-ITS, the typical age was 1.55 rising up to 2.5 sec until the next RTCM message arrives.

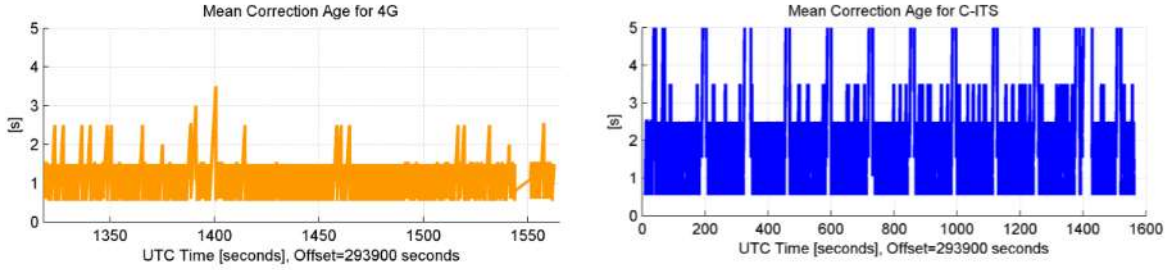

Figure 37: Latency of RTCM delivery for 4G (left side) and C-ITS (right side).

Figure 38 shows the data of the static C-ITS tests in more detail. One can see two effects: the aforementioned increased data latency of one second in average and data gaps in a regular interval of approximately 132 seconds, where for approximately 15 seconds no RTCM messages were received.

The analyses showed that the architectural design of the C-ITS demonstrator was leading to the observed effects. The gaps were a result of the data link between the central computer with the NTRIP client and the RSUs, which had to pass several firewalls. Since the minimum data age was the same for both 4G and C-ITS (time resolution of 0.05 seconds), we are currently convinced that the architecture can be optimized for a deployment at production stage to reach a comparable latency. The influence of the delay on the position solution is discussed in section 5.3. In summary, the 15 seconds gap cause a decrease in the GNSS localization accuracy, while the additional latency did not cause any problem. Hence, in section 5.3, the data analyses were split into data with nominal latency (3 seconds) and data with large latency.

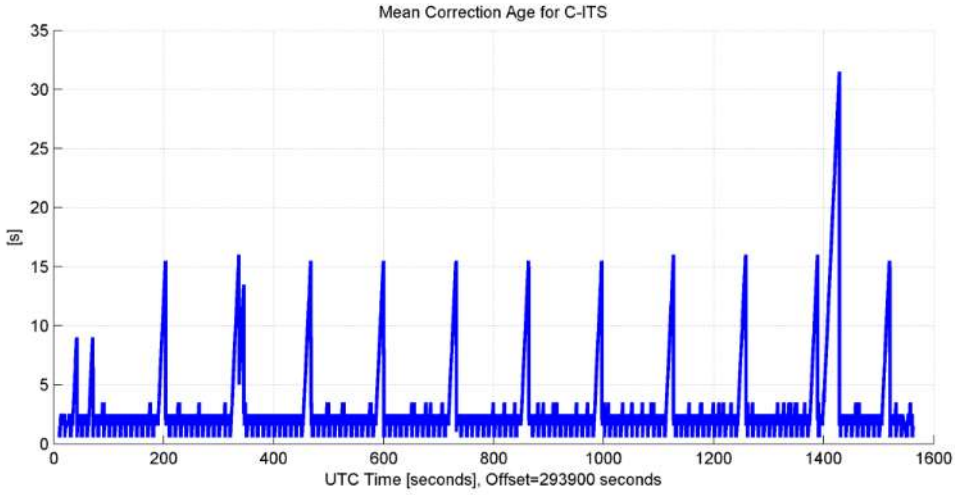

Figure 38: Detailed view on the latency of RTCM delivery for C-ITS

5.3. Analysis of the end user localization system

Within this section, the GNSS data analyses are presented comparing RTK position solutions from two Septentrio Mosaic X5 receivers when receiving RTCM messages via C-ITS and RTCM messages via 4G. The setup is explained in more detail in section 5.2.

Figure 39: Vehicle setup.

The errors of the solutions are calculated by building differences to a reference solution. Therefore, a tactical-grade iMAR iNAT-FSLG-01 GNSS/IMU system was additionally installed in the vehicle.

The analyzed errors are shown in the following figures and tables: Figure 40 shows the cumulative distribution function (CDF) of the horizontal (2D) position errors, Table 8a their 95 and 99.5% percentiles together with the availability of positions with errors below 10 and 20 cm, and Table 8b the percentages of position types obtained. From the tables and figures we see that the percentage of RTK-fixed solutions is very high in both approaches (98.78% and 98.90% when using 4G and C-ITS, respectively) and that their accuracy is comparable, with errors below 10 cm more than 99% of the time. This implies that the additional latency of C-ITS did not significantly affect the accuracy. For PVT solutions with errors above 10 cm, the reliability of the receiver is very good always reporting a correct (overbounding) error estimate when applying a factor of 2.5 to the standard deviation.

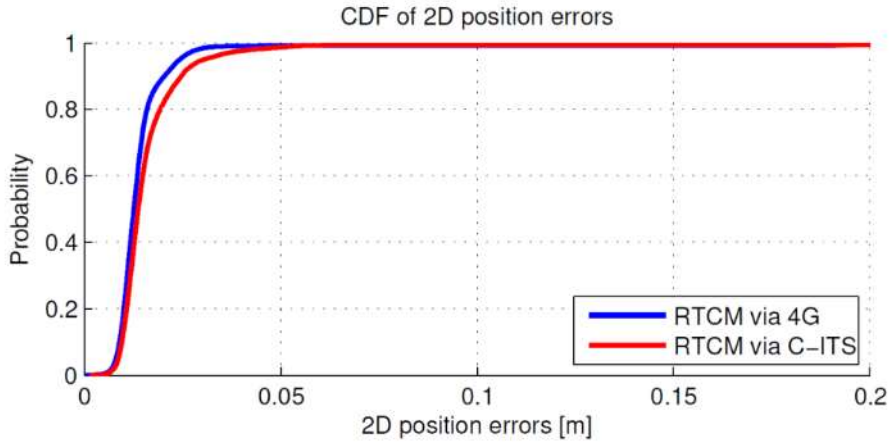

Figure 40: CDF of 2D position errors for both solutions.

Sol.	95%	99.5%	≤ 10 cm	≤ 20 cm
4G	2.4 cm	37.9 cm	99.2 %	99.3 %
C-ITS	3.1 cm	43.4 cm	99.4%	99.4 %

(a) 2D position error statistics

Sol.	No fix	SPP	RTK Float	RTK Fix
4G	0.42 %	0.44 %	0.35 %	98.78 %
C-ITS	0.39 %	0.45 %	0.25 %	98.90 %

(b) Occurrence of position types

Table 8: Horizontal errors and occurrence frequency of position types.

Some issues in our setup allowed us to investigate the impact of the mean RTCM "correction" message age on the position accuracy. Figure 41 shows the observed 2D position error against the mean RTCM message age associated to RTK-fix and RTK-float solutions, respectively. The errors typically encountered in urban and suburban situations are those corresponding to a few seconds delays. The figures also show the influence of older RTCM messages (> 5 seconds) on the RTK solution in our experiments (mostly for highway and rural road conditions). As long as an integer fix was possible, the 2D position error stayed below 20 cm up to 50 sec, which was not expected. For float solutions, it can stay as good as 50 cm if the initial float solution is stable, otherwise, the errors can be as large as 22m (maximum observed horizontal error of a float solution).

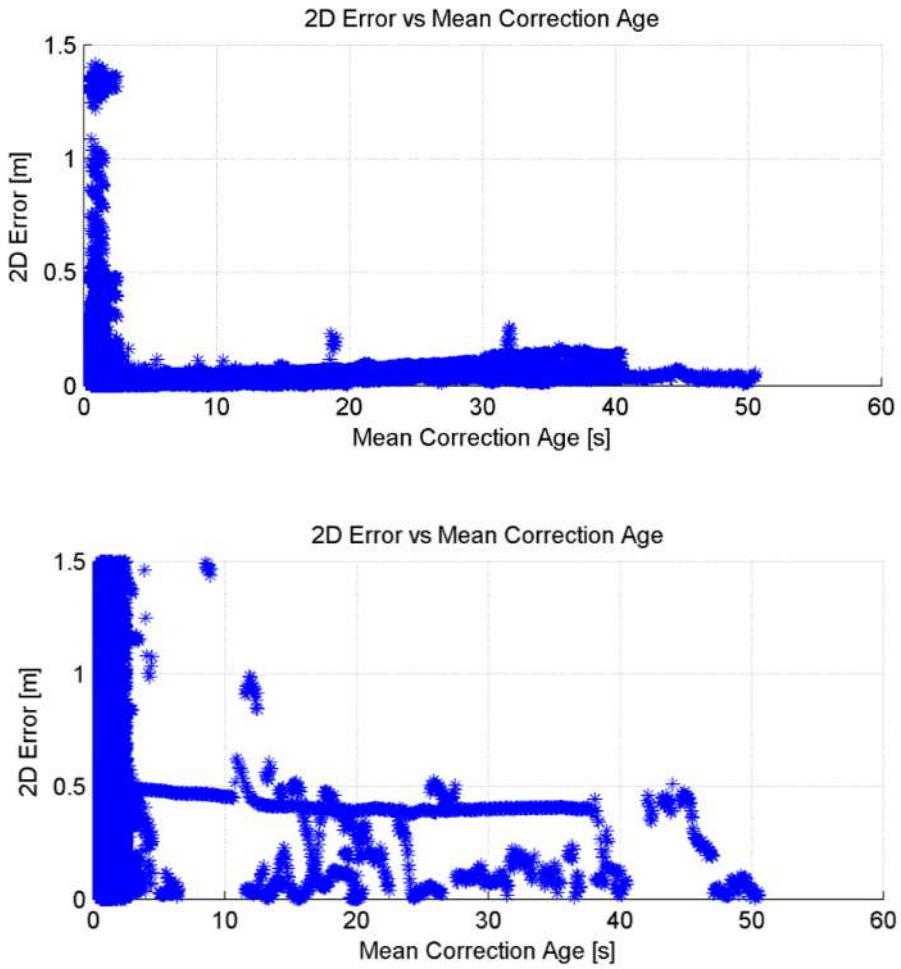

Figure 41: Influence of the mean RTCM message age on the achievable 2D position accuracy.

While in section 5.2 the delay of the RTCM messages was analyzed, there is also a time gap between the GNSS receiver getting the first set of messages until the first RTK solution can be generated. Within our tests, a time difference between the reception of the first and last required RTCM message (block of messages for one epoch) was between 0.05 and 0.1 seconds. The time span

between the last RTCM message and the first fixed RTK solution was between 0.25 and 0.45 seconds. There was always an immediate change from a SPP solution to a fixed RTK solution without a float RTK solution in between.

Summarizing, in theory, a GNSS RTK solution requires continuous RTCM data and a little data delay. Our short-scale experiment showed that the Septentrio Mosaic X5 was able to bridge gaps in the RTCM data of several seconds without a significant decrease in the positioning accuracy with respect to our localization requirements, and larger gaps of up to even 50 s with errors below 20 cm as long as the receiver had a good and fixed RTK solution at the beginning of the gap. The tests further showed that a mean RTCM data delay of 0.55 or 1.55 seconds lead to almost the same accuracy. This robustness against small coverage gaps increases the usability and suitability of RTK for high-accuracy positioning in automotive applications using both, 4G and C-ITS data links. The horizontal position errors observed in our tests were below 10 cm for more than 99% of the time using either 4G or C-ITS as long as a data link was present, and the transmission delays remained reasonably small. Gaps of a few seconds can be bridged by modern mass-market GNSS receivers like the used Septentrio Mosaic x5 while still maintaining a significant accuracy (better than 10 cm in our tests). For gaps of up to 50 s, an error ≤ 20 cm could be achieved under specific circumstances. In addition to confirming the feasibility of using C-ITS for RTCM message delivery, this relatively large tolerance to communication delays enables the use of different and complementary data links for the delivery of the necessary RTCM corrections and lowers the barrier to the spreading of RTK positioning for high accuracy in automotive applications.

The ESRIUM use case 3, the provision of GNSS-correction data provision with C-ITS messages, was implemented in Austria by a prototype consisting of a highway track with C-ITS infrastructure connected to a commercial EGNSS RTK provider and an automated vehicle. It was demonstrated that the generic concept of transmitting EGNSS RTK correction data via C-ITS works as concerns the provision of the data, the transmission of the data and the reception and processing of the data in the vehicle. The location accuracy that is achieved in the vehicle is 10 cm and judged to be sufficient for automated driving.

It was shown that all needed transmission formats from the EGNSS RTK source to the transmission point are already - or are in the process of being - standardized, are therefore readily implementable and that, in Austria at least, an EGNSS RTK source is commercially available. The prototype was implemented on C-ITS infrastructure currently being deployed on the entire Austrian highway network, which adds to the confidence in this result, though some observations appeared which could not be resolved within the scope of the project.

The observed prototype position accuracy in the vehicle using EGNSS RTK over C-ITS was 10 cm. The projected achievable operative position accuracy in the vehicle using EGNSS RTK over C-ITS was determined to not be able to exceed that, so also 10 cm. This compares to 300 cm (3 m) using EGNSS without RTK. It also compares to 2 cm theoretically achievable with the EGNSS RTK prototype source EPOSA. A maximum error of 10 cm in 99.4% of cases is deemed sufficient for Automated Driving by project partner Virtual Vehicle, who have provided the automated car functions for the project.

The software in the road side units which relays the RTK messages from the RTK source to the moving vehicles was implemented as a wrapper rather than integrating it into the software core. This resulted in a pulsating transmission characteristic as opposed to a precisely timed process. Still this did not compromise the precision and also allowed for testing of the vehicle client in the case of uncharacteristic transmission behavior, which was successful.

Further investigation should include a large scale test and focus on the effect of gaps in transmission coverage.

Details of the implementation are provided in the ESRIUM Deliverable D3.5 "Report on extension of C-ITS by EGNSS use case".

SECTION 6: GALILEO OSNMA UNDER REAL-WORLD SPOOFING

During a national jamming and spoofing event organized by the Austrian Ministry of Defense (AMOD), it was possible to investigate the behavior of the Septentrio Mosaic X5 GNSS receiver under spoofing using different Galileo OSNMA configurations (OSNMA off, loose, strict). Therefore, a spoofer (developed and operated by a third party) was configured to spoof signals on GPS L1 C/A and Galileo E1B/C for all satellites above 10° elevation. The tests were executed on September 7th 2023.

Unfortunately, the test execution was suboptimal: the spoofing signal was transmitted with too much signal power. Hence, it was more a jamming than a spoofing and the receiver lost track of the signals. The fact that it was more a jamming than a spoofing (cf. Figure 42) was also most probably the reason, why the spoofing did not work in any case. Nevertheless, some conclusions are possible, which will be explained in the next paragraphs.

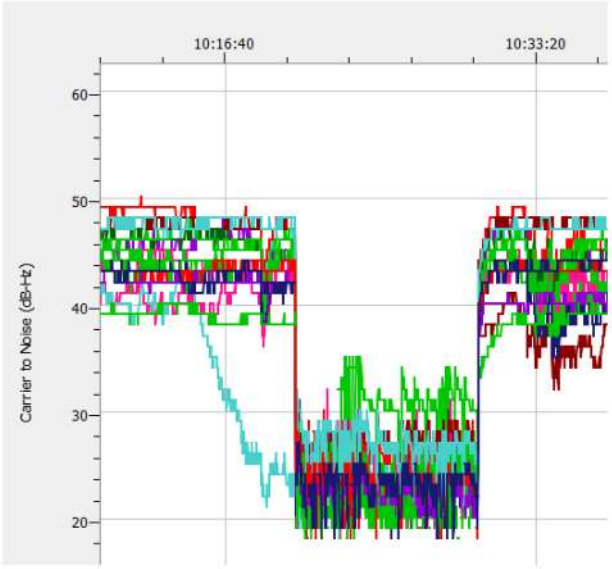

Figure 42: Effect of too powerful spoofing on the carrier to noise ratio.

In Figure 43, one can see that the position standard deviation immediately drops when the powerful spoofing is activated. The GNSS receiver solution drops from RTK-fixed (PVT Mode, light green bar) to stand-alone (dark-blue bar) and the standard deviation is untypically high (also for a stand-alone solution). This is unexpected since the spoofer was only on L1/E1 while the GNSS receiver unintentionally was configured to use L1/E1/L5/E5. Hence, one conclusion of the test is that also single frequency attacks can cause serious effects on modern multi-frequency GNSS receivers. The authors assume that within the receiver design, L1/E1 still has more weight compared to the other bands due to historical reasons (L1 was the first frequency and hence it is always available) as well as due to the fact that the L1/E1 band is the only band reserved solely for GNSS, while L2/L5/E5/E6 is a shared band.

To see, whether a GNSS receiver configured for L1/E1 only would react differently, it was tried to post-process the L1/E1 data only but the measurement data was not usable at all (the signal to noise ratio was too bad due to the strong signal from the spoofer).

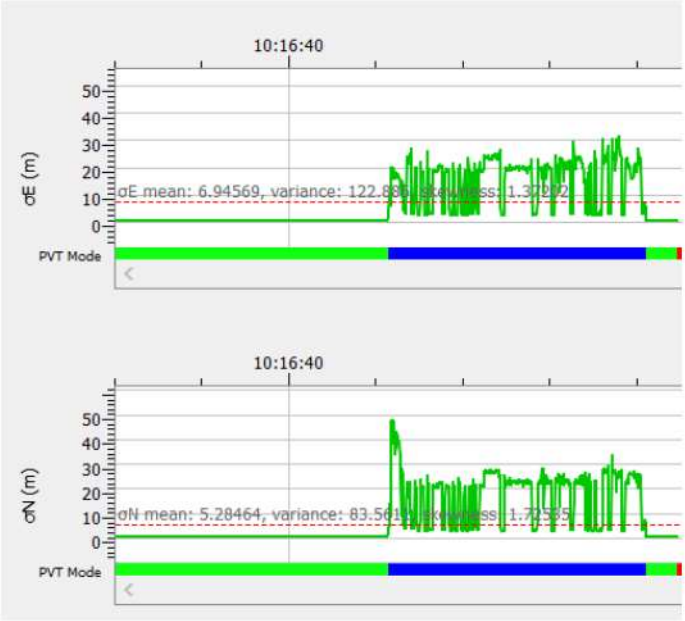

Figure 43: Effect of spoofing on the east (upper part) and north (lower part) standard deviation.

In general, the Septentrio Mosaic x5 receiver has implemented algorithms to detect interference/jamming and spoofing (methods unknown). During all transmissions, the receiver detected interference, but only with Galileo OSNMA in strict mode, it detects spoofing (will be explained later).

In Figure 44, again, one can see the receiver behavior during spoofing. The spoofing transmission is indicated by the yellow bars. During the first spoofing, the GNSS receiver was configured in OSNMA off mode (the same behavior was observed for the OSNMA loose mode), while during the second spoofing it was configured in OSNMA strict mode (only taking authenticated Galileo satellites).

Figure 44: Effect of spoofing.

In both cases, the Septentrio Mosaic X5 immediately falls back to SPP (Stand-Alone) when spoofing starts (blue bar). Between the first and the second spoofing, the GNSS receiver configuration was changed to OSNMA strict. Hence, the receiver needed a short period to authenticate the Galileo satellites. In this time, no position solution was available (red bar in the PVT mode). In the following paragraph, the data is analyzed in more detail for the OSNMA strict mode.

As soon as the spoofing starts, the GNSS solution falls back to stand-alone mode. For the first 4 minutes, the receiver continued using the authenticated Galileo navigation messages from before. Within these 4 minutes, the receiver detected interference, but did not detect spoofing, because the receiver did not have new navigation messages. The receiver was not able to decode the manipulated navigation messages created by the spoofer (most probably because of the bad signal-to-noise ratio). After 4 minutes, the receiver was able to decode the navigation message from the spoofer without correct OSNMA Navigation bits. Hence, the authentication process failed (the satellite status changed

from “authentic” to “unknown” and later partly to “authentication failed” and the receiver assumes a spoofing attack and refuses a PVT output. It is not known what logic is implemented by Septentrio, and there is also no specific logic defined in the Galileo ICD. Nevertheless, when suddenly, all Galileo satellites lose their authentication status, one can assume that something unusual is going on. When the spoofing attack was over, for the next 2 minutes, the receiver still indicated spoofing because still no authenticated navigation messages from the satellites were available. After about two more minutes, the receiver was able to decode and authenticate the navigation messages from the satellites and started again outputting an authenticated PVT solution.

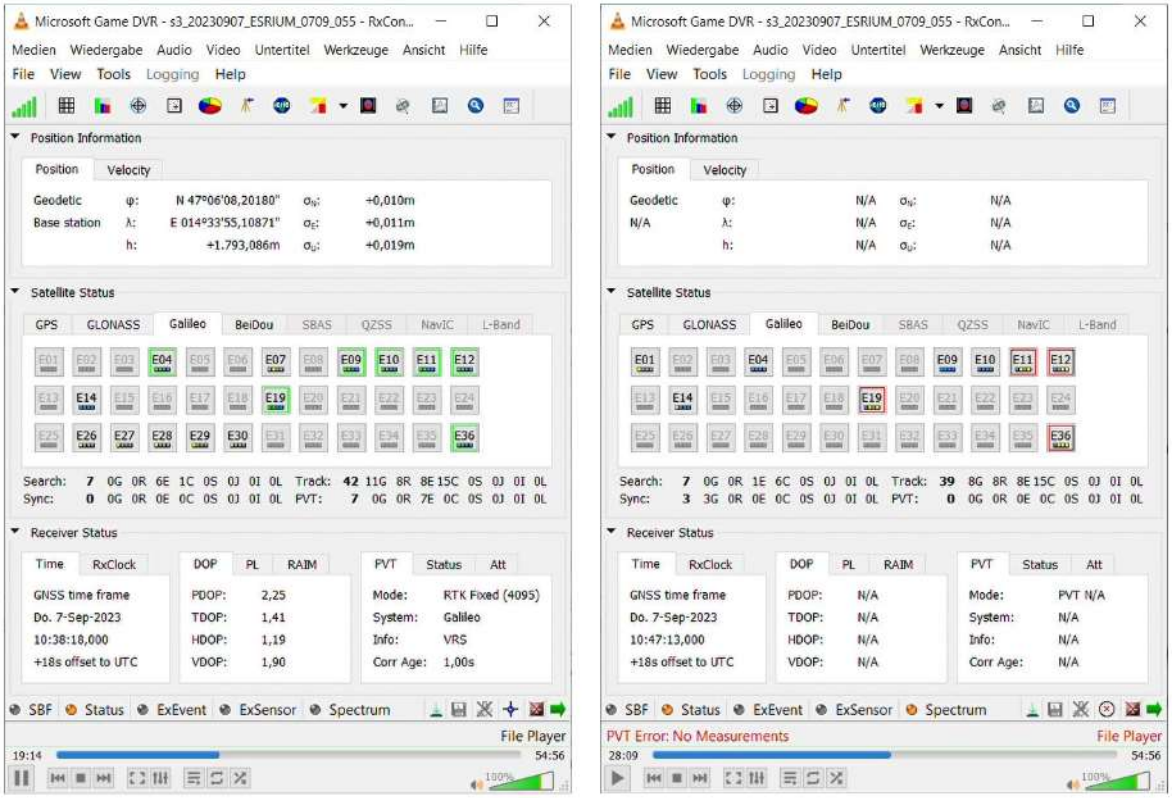

Figure 45: Septentrio User Interface.

Figure 45 shows the Septentrio User Interface (RxControl) with green boxes for authenticated satellites and red boxes for satellites where the authentication failed. No boxes tell that the status is unknown.

ATTACHMENT 1: INTERACTIVE MAPS

As described in section 2.3 interactive maps are attached to this report. The list of map-files and the corresponding test conditions are listed below.

desired vehicle velocity [km/h]	interactive map file
90	• Test run_01.html • Test run_03.html • Test run_04.html
110	• Test run_05.html • Test run_06.html • Test run_07.html
130	• Test run_08.html • Test run_09.html • Test run_10.html

The corresponding interactive files are available publicly from the following permanent Zenodo Link:

Solmaz, S. (2023). Interactive maps for the visualization of ESRIUM automated driving tests with various EGNSS localization solutions (Version 1) [Data set]. Zenodo. https://doi.org/10.5281/zenodo.10221769